metals

MDPI

Article

Study of Electrochemical and Biological Characteristics of As-Cast Ti-Nb-Zr-Ta System Based on Its Microstructure

Mariana Correa Rossi [1,*], Beatriz Navarro Ventura [1], Lara Milián [2,3], Angel Vicente Escuder [1] and Vicente Amigó Borrás [1]

[1] Instituto de Tecnología de Materiales, Universitat Politècnica de València, 46022 Valencia, Spain; beanaven@etsii.upv.es (B.N.V.); avicente@mcm.upv.es (A.V.E.); vamigo@mcm.upv.es (V.A.B.)
[2] Faculty of Medicine and Dentistry, Universitat de Valencia, 46010 Valencia, Spain; lara.milian@uv.es
[3] Incliva Biomedical Research Institute, 46010 Valencia, Spain
* Correspondence: mariana.rossi@unesp.br

Abstract: The quaternary Ti-Nb-Zr-Ta (TNZT) alloy was successfully cast-fabricated with the objective to be used in the medical field. Samples' microstructure was compared to CP-Ti and Ti-6Al-4V (control samples) and related to corrosion, ion release and biological properties. As-cast TNZT was formed with large β grain sizes (285 μm) compared to the ultrafine α grain sizes of CP-Ti (11 μm) and the α + β ultrafine grain sizes of 1.45 μm and 0.74 μm. Hardness and flexural elastic moduli (94 HV and 43 GPa) came close to the biological structures, such as dentin and enamel values. The ion release mechanism of as-cast TNZT was significantly lesser than CP-Ti and Ti-6Al-4V, which can be related to the difference in samples' grain sizes and chemical compositions. However, the corrosion rate was higher than for the control samples; this way offers corrosion properties inferior with respect to the properties obtained in the reference materials. Biological assays demonstrated that the two-cell (hDPSCs and MG-63) lineage studied presented good adhesion and capability to differentiate in bone cells on the as-cast TNZT surface, and no cytotoxicity effects were found. Details and reasons based on samples' microstructure are discussed.

Keywords: β-Ti alloy; corrosion resistance; biocompatibility; biomedical materials

Citation: Rossi, M.C.; Ventura, B.N.; Milián, L.; Escuder, A.V.; Amigó Borrás, V. Study of Electrochemical and Biological Characteristics of As-Cast Ti-Nb-Zr-Ta System Based on Its Microstructure. *Metals* **2022**, *12*, 476. https://doi.org/10.3390/met12030476

Academic Editors: Lin Mao and Xiaobo Zhang

Received: 12 February 2022
Accepted: 7 March 2022
Published: 11 March 2022

1. Introduction

Dental implants, like teeth, emerge from the bone through oral soft tissue into an oral cavity that serves as a shelter for a wide variety of microorganisms and, thus, peri-implantitis can occur. Peri-implantitis is defined as the inflammatory process that affects the tissue surrounding dental implants, caused by the presence of different types of bacterial species.

Titanium (Ti) and its alloys are used in dentistry for manufacturing implants, prosthetics and prosthetic components for their favorable mechanical, physical and chemical properties, of which low density, high mechanical strength, good corrosion resistance and, therefore, biocompatibility have promoted their application in the biomaterials field since 1951 [1].

New-generation aluminum (Al) and vanadium (V) alloys present an elastic modulus insofar as natural bone can generate disuse atrophy due to the stress shielding phenomenon, which can then lead to implant failure [2]. Studies have shown that the release of these ions (present in the most widely used dental implants) is cytotoxic for the body, and can promote neurological conditions like Alzheimer's disease [3]. Thus, developing new materials free of toxic metals has emerged with biological improvements and better mechanical compatibility (lower elastic modulus, a value closer to that of bone). Considerable interest is being shown in developing and improving Ti alloys for their high strength-toughness combination. Alloys that introduce niobium (Nb), zirconium (Zr) and/or tantalum (Ta) are believed to be the most promising [4].

In more detail, Zr is considered a neutral element in Ti binary alloys but is considered a β-stabilizing element when it forms part of Ti alloys containing Nb and/or Ta (isomorphic-type β stabilizers) [5]. It is a chemical element with atomic number 40 and is located in group 4 on the periodic table and, thus, corresponds to the same group as Ti, which is why they have similar properties. It is a hard corrosion-resistant metal with very flattering esthetic characteristics in dentistry [6]. For this reason, more similar elastic properties to bone tissue are sought, with greater biomimicry and biocompatibility over time. This is achieved with the well-known hyperelastic alloys which, in addition to Ti and Zr, add other metals like Nb (Min Kim et al., 2020) [7]. This element is in group 5 of the periodic table and is a ductile metal. When Nb joins Ti and Zr to form this alloy, a metal is generated with Young's modulus close to that of the supporting bone (71 GPa). The yield stress of this alloy is 687.03 MPa, very close to 680 MPa for Ti-6Al-4V [6]. Several studies [8–10] have demonstrated that the Ti-Nb-Zr system offers good biomechanical behavior when subjected to new heat and surface treatments, as well as good biocompatibility. Their response is also considered optimal when subjected to the addition of Ta. Similar to Nb, it is a chemical element in group 5 of the periodic table and is used in dental and surgical fields for its chemical inertness and slow oxidation in alkaline solutions [11].

These implants' long-term success and prosthetic structures will depend on their resistance to the forces that result from chewing, and to chemical and electrochemical reactions that occur on surfaces in the environment.

An extremely wide variety of scientific articles mechanically characterized this alloy. Theoretical data about its elastic modulus and resistance are known, yet statements are scarce and hypotheses increase when focusing on the microstructure's effects on biological and electrochemical properties. This is why, after its in-depth mechanical analysis, it must give way to its in vitro analysis to obtain a complete alloy characterization and to know if it is as promising as believed or not.

Different as-cast materials have been studied for biomedical applications as Ti-12Mo-xNb, with non-post processing procedures that were investigated for the effect of Nb content on β-Ti alloy in hardness, and the elastic modulus related to the β phase content [12]. In the work of Ma et al., 2021, different β-Ti alloys fabricated by as-cast omitting post processing procedures to reduce costs production [13] were studied, as well as in the work of Rodrigues et al., 2021, which studied a novel as-cast Ti-Mo-Zr alloy with high β phase content, also for biomedical application [14]. However, there is a lack of electrochemical information about the as-cast β-Ti alloys with non-post processing procedures. For this purpose, the present work focused on investigating some clues as to how the microstructure and alloy composition may affect cellular properties, ion release and corrosion resistance when the as-cast Ti-Nb-Zr-Ta quaternary system comes into contact in a biological environment.

Ternary Ti-Nb-Zr alloys have been studied for their use in dentistry, with quaternary Ti-Nb-Zr-Ta ones mainly in the medical field [15].

Infiltration of saliva between implants and implant-supported structures creates galvanic cells between dental alloys that promote corrosion by cracks, which then lead to an ion release. In addition, fluoride ions can etch the oxide layer on the surface of Ti and its alloys by decreasing these metals' corrosion resistance [15].

Interactions between these fluoride ions and alloy metals are interesting because of the increasing use of compounds containing high fluoride levels to prevent tooth loss. When these compounds are present in toothpastes, gels and/or mouthwashes, possible corrosion products can induce inflammatory reactions and periprosthetic bone loss [12,15]. Consequently, one of the purposes of such studies is to evaluate the surface response of the Ti-Nb-Zr-Ta based on grain size and β phase content after long-term immersion in artificial saliva and to analyze the release of metal ions, electrochemical properties and biological effects when in contact with cells using saliva artificial electrolytes.

2. Materials and Methods

As-cast Ti-Nb-Zr-Ta (35 wt% Nb, 7 wt% Zr and 5 wt% Ta) were supplied by the TOSOH company (Tokyo, Japan) in a cast state as a 2 kg ingot to obtain bars measuring 2.8 cm × 26.5 cm. The CP-Ti and Ti-6Al-4V samples were used as a reference. Before the characterization of alloys, specimens were obtained in the desired size and shape for each study. For this purpose, an Accutom 10/100 Struers model (Madrid, Spain) precision metallographic cutter was employed, equipped with a 357CA diamond blade. Subsequently, some specimens were subjected to metallographic preparation by using the Struers LaboPress-3 and Buehler transoptic clear powder resin 20-3400-080. Then they were embedded with transparent resin methacrylate (PMMA), followed by chemical etching. The process parameters were: 15 kN force, 180 °C of temperature, 7-min heating and 7-min cooling. To remove the samples' surface layer, they were sanded by coming into direct contact with 220, 500 and 1000 mesh sandpaper (abrasive material). This was performed by a Struers LaboPol-21 roughing machine at a speed of 150 rpm. Finally, specimens were polished by a Struers LaboPol-5 machine to obtain the desired smooth and shiny surface finish. Abrasive solutions were 9 µm water-based diamond suspension and 0.04 µm OP-S solution (colloidal silica suspension). Finishing was done at 150 rpm and 15 N for 6 min.

Phase quantification, along with lattice parameter, crystallite size, lattice strain and grain size, were studied and analyzed by the following techniques:

(1) X-ray diffraction by a Bruker's Phaser model 2D X-ray diffractometer (Karlsruhe, Germany) operating at 30 kV and 10 mA using the Cukα wavelength of 1.5405 Å. The sweep over the sample was carried out from 20° to 90°. Data were obtained and processed with the diffractometer's integrated software and version 2.94 of the MAUD (Material Analysis Using Diffraction) (Trento, Italy) software, and the OriginPro 8.5 software (Northampton, MA, USA) [16].

(2) The AURIGA compact field emission scanning electron microscope (FIB) (Jenoptik, Jena, Germany) was utilized with an Orsay physics scattered electron detector (BSE) and a Kleindiek X-ray detector (EDS) (ZEISS-ULTRA 55, Oberkochen, Germany).

(3) An Oxford Instruments backscattered electron detector (EBSD) (Symmetry, Oberkochen, Germany) was used to obtain information about the as-cast TNZT crystalline structure. First, samples were prepared by metallographic techniques and a final polish, prior to the analysis, for approximately 5 h with nondried OP-S solution in a vibratory polisher (Struers-Labopol-5). Analyses were carried out in an Aztec HKL Max system (Wiesbaden, Germany). Samples were placed at an inclination of 70° in relation to the detector (Symmetry S2®) (Wiesbaden, Germany) at an acceleration voltage of 20 kV. Three possible phases were selected to be analyzed: β-Ti, α-Ti, martensite α″-Ti. Patterns were analyzed by the HKL Channel 5 (Oxford Instruments) software (Wiesbaden, Germany).

Mechanical properties were evaluated for the 4-point bending test using a Shimadzu universal testing machine, model AG-100kN Xplus.

Bending strength (σ_B) and elastic modulus E_B were calculated using Equations (1) and (2), where P is the applied load, b and h are respectively the specimen's width and thickness, L and l are the distances between the lower (22 mm) and upper (11 mm) loading rollers, and f is sample deflection.

$$\sigma_B = \frac{3P(L-1)}{2wt^2} \quad (1)$$

$$E_B = \frac{Pa\left(3l^2 - 4a^2\right)}{f4bh^3} \quad (2)$$

For this study, the employed samples were 22 mm long, 11 mm wide, and 4 mm thick. The main objective was related to the stresses and strains that occurred at the maximum and breaking points. Furthermore, the elastic modulus ($E_{flexural}$) was determined according to the spacing between supports and specimen thickness. The force was applied at two

points on the specimen and its magnitude was 100 kN. The distance between the centers of supports was 25 mm.

The elastic modulus was also evaluated by KARL DEUTSCH model 1090 ultrasonic Flaw Detector ECHOGRAPH 1090 equipment (Wuppertal, Germany), which comes with a portable monitor and several functions to display information. Data were obtained by recording the sample itself with two probes: the first used longitudinal waves and the second transversal waves. The elastic modulus was determined from the speed of ultrasonic pulses. Contact between the sample and both probes was achieved using coupling grease that worked as conductive fluid.

With this information, the round-trip distances of the echo of ultrasonic pulses (gates) were measured. To obtain the best possible results, a fourth echo was taken and divided by 4. Analyzing the thickness between peaks gave the material's longitudinal and transverse rate values.

The hardness was obtained using a load of 147 N by the Rockwell method (BECLA), with a spherical steel indenter of 1/16″ diameter. A total of $n = 5$ measures were made for each sample. Then the data found were converted to Vickers hardness.

A metal ion release test was carried out for as-cast TNZT, and the CP-Ti and Ti-6Al-4V samples, as controls. It comprises the first step to measure cytotoxicity. First, specimens were cut, subjected to metallographic preparation, and sterilized. The size of the metallic samples was 1.5 cm^2 and the contact surface was 0.744 cm^2 for all the samples. Once specimens were prepared, a nontoxic electrolyte was required, denominated Ringer-Hartmann and composed of NaCl (5.97 g/L), KCl (0.37 g/L), $CaCl_2$ (0.22 g/L) and $C_3H_5O_3xNa$ (3.25 g/L) in which they were deposited to evaluate the ion release. This is one of the means to measure the samples' cytotoxicity.

It was necessary to simulate oral environment conditions to generate an adequate ion release for our needs. To do so, the half-life of a dental implant was investigated (between 15 and 25 years). Brushing conditions were simulated for 20 years with an average of 2 brushings/day. This corresponded to incubation in 50 mL of electrolyte (artificial saliva) with each sample prepared for 732 h (30 days and 12 h) at 37 °C. The pH of the modified Ringer-Hartmann artificial saliva was 6.53, which is an acidic pH (<7) that favors the release of ions, and it was similar to the oral environmental pH. Ion release tests were run for each alloy in triplicate. To quantify the ion release from the alloy (Ti, Nb, Zr and Ta), liquids were taken to be analyzed by atomic absorption spectroscopy of hardened plasma coupling (ICP-OES) (Varian, model 715-S, Jena, Germany). The wavelengths to determine the content of the ions released to the solution were 336.0 nm (Ti), 313.1 nm (Nb), 343.8 nm (Zr) and 263.5 nm (Ta).

In order to characterize the electrochemical processes that occur when as-cast TNZT alloys are subjected to environments, potentiodynamic corrosion tests were carried out in the oral environment at 37 °C in modified Ringer-Hartmann artificial saliva heated at 37 °C and kept constant by the thermocouple. The sample surface areas (0.784 cm^2) were exposed during tests. For the analyses, three electrodes were used in the electrochemical cell (Ag/AgCl, as the reference electrode; platinum (Pt) as auxiliary and the sample as work electrode) and measurements were carried out by using the Metrohm potentiostat (model PGSTAT204) (Utrecht, the Netherlands). The corrosion rate was determined by Tafel's extrapolation methods. Cathodic (β_c) and anodic (β_a) Tafel slopes and corrosion current densities (i_{corr}) were estimated from Tafel plots. The corrosion potential was also established. Three repetitions of all the tests were performed at a scan rate of 2 mV/s. Polarization resistance (R_p) was calculated based on the Butler–Volmer [17] equation by taking the inverse of the slope of the current density-potential curve at corrosion potential as follows:

$$i = i_{corr\left(e^{2.303\left(\frac{\eta}{\beta_a}\right)} - e^{2.303\left(\frac{\eta}{\beta_c}\right)}\right)} \quad (3)$$

The overpotential, η is defined as the difference between applied potential and the corrosion potential E_{corr}. The E_{corr} is the open-circuit potential of a corroding metal. The

corrosion current, i_{corr} and the Tafel constants (β_a and β_c) were measured from the experimental data.

For small η when potentials are close to corrosion potential, the Butler–Volmer equation can be reduced to:

$$i_{corr} = \frac{1}{2.303} \frac{\beta a \beta c}{(\beta a + \beta c)} \left(\frac{1}{R_p}\right) \quad (4)$$

Then, rearranged, the equation R_p is given by:

$$R_p = \left(\frac{\beta a \beta c}{(\beta a + \beta c)\ (i corr)}\right)\ \left(\frac{1}{2.303}\right) \quad (5)$$

The cell types used in the biological tests were primary human dental pulp stem cells and the human cell line from osteosarcoma MG-63. The former was isolated from the third molar from different donor patients. The latter came from the American Type Culture Collection (ATCC CRL-1427, Barcelona, Spain) from adult donors (see Figure 1). hDPSCs cells were cultured in α-MEM culture medium (Thermo Fisher Scientific, Paisley, UK), supplemented with 10% fetal bovine serum (FBS) (Thermo Fisher Scientific, Paisley, UK); 1% penicillin/streptomycin (P/S) (Thermo Fisher Scientific, Grand Island EEUU); 1% L-glutamine (EuroClone, Pero, Italy); and 1% amphotericin B (Thermo Fisher Scientific, Paisley, UK). MG-63 cells were cultivated in MEM culture medium (Thermo Fisher Scientific, Paisley, UK) and supplemented with 10% FBS; 1% penicillin/streptomycin (P/S); 1% L-glutamine; 1% nonessential amino acids (NEAA) (Thermo Fisher Scientific, Paisley, UK); and 1% pyruvate (Thermo Fisher Scientific, Paisley, UK).

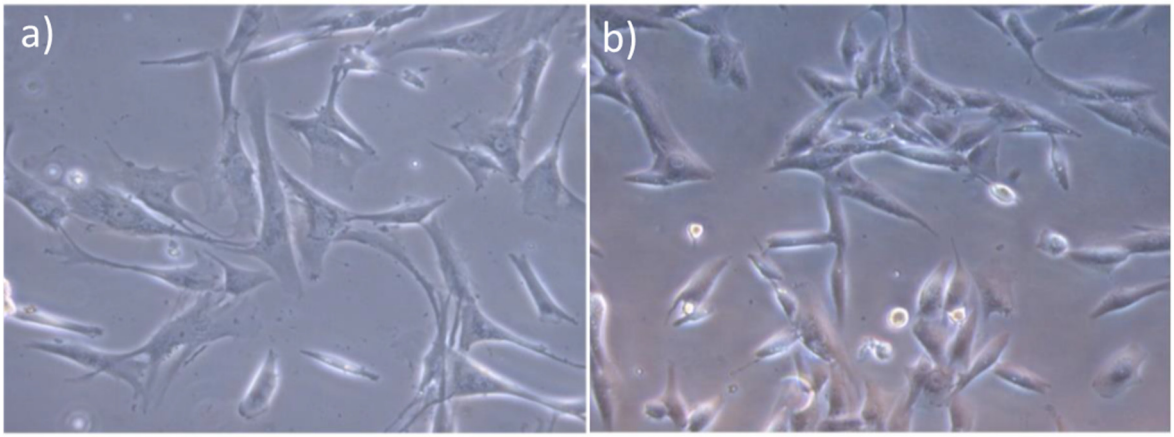

Figure 1. (**a**) hDPSCs and (**b**) MG-63 cells. 40×.

The composition of the osteogenic differentiation assay was as follows: α-MEM supplemented with 10% FBS, 1% P/S antibiotic solution, 2 mM of L-glutamine, 10 µg/mL of glycerol-2-phosphate (Merck; Darmstadt, Germany), 4 µg/mL of ascorbic acid (Merck; Germany), 0.1 µg/mL of dexamethasone (Merck; Germany) and 50 ng/mL of BMP-2 (Stem Cells Technologies; Saint-Egrève, France). Before the experiments, samples were immersed in an ELMA ultrasound bath in a glass beaker with ethanol for 10 min at room temperature to be sterilized. This consists of injecting saturated and dry steam under pressure in an atmosphere between 12 °C and 134 °C, into which samples were introduced. To prevent contamination, before starting the biological assays, samples were placed in Petri dishes at a distance of 20 cm in relation to ultraviolet light for 1 h.

The MTS protocol was followed for the cytotoxicity assays. Briefly, MG-63 and hDPSCs cells were seeded in triplicate in a 96-well plate at a density of 1×10^4 cells/well. After 24 h, the culture medium was replaced with the corresponding dilutions of the saliva obtained in the ion release assay at different concentrations (see Table 1) and cells were cultured for 48 h. After the conditioned media treatment, an MTS (Sigma-Aldrich; Madrid, Spain) assay was carried out. For that purpose, 20 µL of MTS reagent were added to each well,

and samples were incubated for 2 h. Then absorbance was detected at 490 nm in a Victor X3 2.030 multilabel reader (PerkinElmer; Waltham, MA, USA). The absorbance value is directly proportional to cell viability. The groups present in each triplicate were as follows: C- (negative control): hDPSCs or MG-63, with α-MEM or MEM red phenol-free medium, respectively; C+ (positive control): hDPSCs or MG-63 cells with latex conditioned medium; BC-(blank from the negative control), red phenol-free medium and cells; Ps% (pure artificial saliva x%): hDPSCs or MG-63 with Ringer-Hartmann modified at x% (1, 10 or 25); BPs% (blank from artificial pure saliva at x%): Ringer-Hartmann modified at x% (1, 10 or 25) and cell-free; Mx% (samples at x%): hDPSCs or MG-63 cells with Ringer-Hartmann modified with ions released from alloys at x% (1, 10 or 25); BMx% (blank of the sample at x%): Ringer-Hartmann modified with ions released from alloys at x% (1, 10 or 25) and cell-free.

Table 1. Preparing artificial saliva solutions at different concentrations for the cytotoxicity analysis.

Dilution of Solutions	Modified Ringer Hartmann (μL)	Red Phenol-Free Culture Medium (μL)
Modified Ringer-Hartmann at 1%	10	990
Modified Ringer-Hartmann at 10%	100	900
Modified Ringer-Hartmann at 25%	250	750

The obtained absorbance results were processed and normalized in relation to the negative control (cells treated with their conventional medium), which is considered 100% cell viability.

Osteogenic differentiation was evaluated by the immunofluorescence detection of osteocalcin (OC) and alkaline phosphatase (ALP). For this assay, 12 samples of each material were required for both cells hDPSCs and MG-63. Samples presented the following measurements: diameter of 5 mm, a thickness of 1 mm and a mass of approximately 0.2 g. Having completely sterilized samples, as previously explained, 8-well culture chambers were used as controls to seed cells on a surface specifically treated for cell growth to compare to the cells seeded on alloys. Then 5×10^3 cells/well were seeded in wells and 7×10^3 cells/well in samples. A specific amount was selected after performing different tests with a variable cell population.

Once cells had reached 30% confluence, the conventional culture medium was replaced with a differentiation medium. While they were incubated in a humidified atmosphere with 5% CO_2 at 37 °C and the culture medium, both proliferation and differentiation media were renewed every 2 or 3 days. For the immunofluorescence analysis, samples were fixed with 4% paraformaldehyde in phosphate-buffered saline (PBS), pH 7.4, for 10 min. Once washed, cells were permeabilized with 0.1% Triton X-100 in PBS for 5 min. After three washes, cells were incubated for 30 min with blocking solution (1% bovine serum albumin (BSA) and 1.1% Tween-20 in PBS). Then cells were incubated with osteocalcin (1:200) for 3 h at room temperature. For the secondary antibody control, two wells/chambers containing only the solvent were used. They were incubated for 1 h at room temperature (in the dark) with a secondary anti-mouse antibody (1:200) and DAPI (1:500). Samples were analyzed using a fluorescence DM 4000D Leica Biosystems microscope (Leica Biosystems; Wetzlar, Germany) and photographed with a Leica DFC 340FX camera. After three washes, cells were incubated with 1:200 secondary anti-mouse antibody fabricated in Saint Louis, MO, USA (D2883 from Merck; Switzerland) for 2 h at room temperature in the dark. After the final washes, nuclei were stained with 4′,6-diamidino-2-phenylindole (DAPI).

3. Results

3.1. Structural and Microstructural Characterization

The XRD pattern shown in Figure 2 indicates the presence of martensitic and body-centered cubic Ti in the α″ and β phases. In the XRD pattern, the peak referring to the $(211)_{\beta}$ plane, located at 2θ = 69.95°, presented greater intensity than the other peaks. Inside the diffraction pattern, the location of the peak referring to α″-Ti $(103)_{\alpha}$, and contained in 2θ = 70.12°, is indicated in more detail. Here, we see that most peaks are related to the β phase.

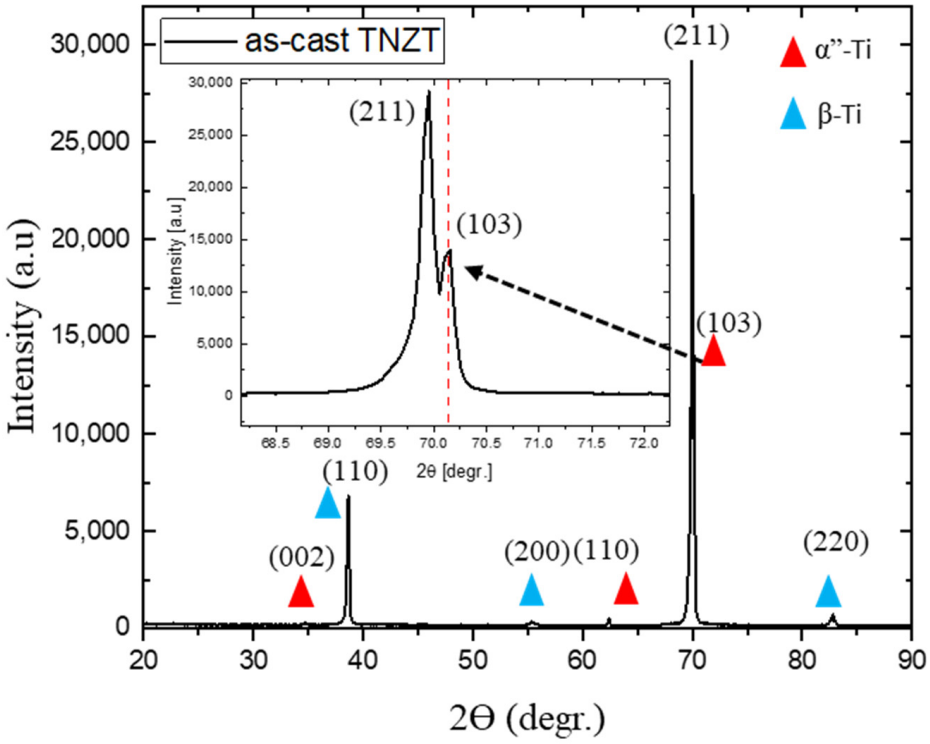

Figure 2. XRD pattern of the as-cast TNZT sample.

The high-magnification SEM images corresponding to the EDS mapping of as-cast TNZT (see Figure 3a–d) further proved the previous inference in the element distribution of Ti, Nb, Zr and Ta. All the elements presented good distribution and homogeneity to one another, and no regions with high concentrations of elements were found. It is well-known that β phase stability can be achieved by the amount of alloy elements, and also by alloy composition. Nb and Ta are two of the most important β-stabilizing elements that strongly influence the phase transformation of Ti alloys. Sufficient Nb and Ta contents can lead to (Ti, Nb), (Ti-Ta) bcc solid solutions. Zr can be considered a neutral element, it does not significantly affect the T_{β} quantity and can be added to metastable β phase Ti alloys. In this case, neutral elements can alter hexagonal isothermal ω phase formation kinetics during aging. However, the role played by Zr as an effective β stabilizer when combined with Nb and Ta is starting to be acknowledged [18]. This can explain the good homogeneity of the elements in the Ti matrix. These data confirm the results obtained by the XRD profiles.

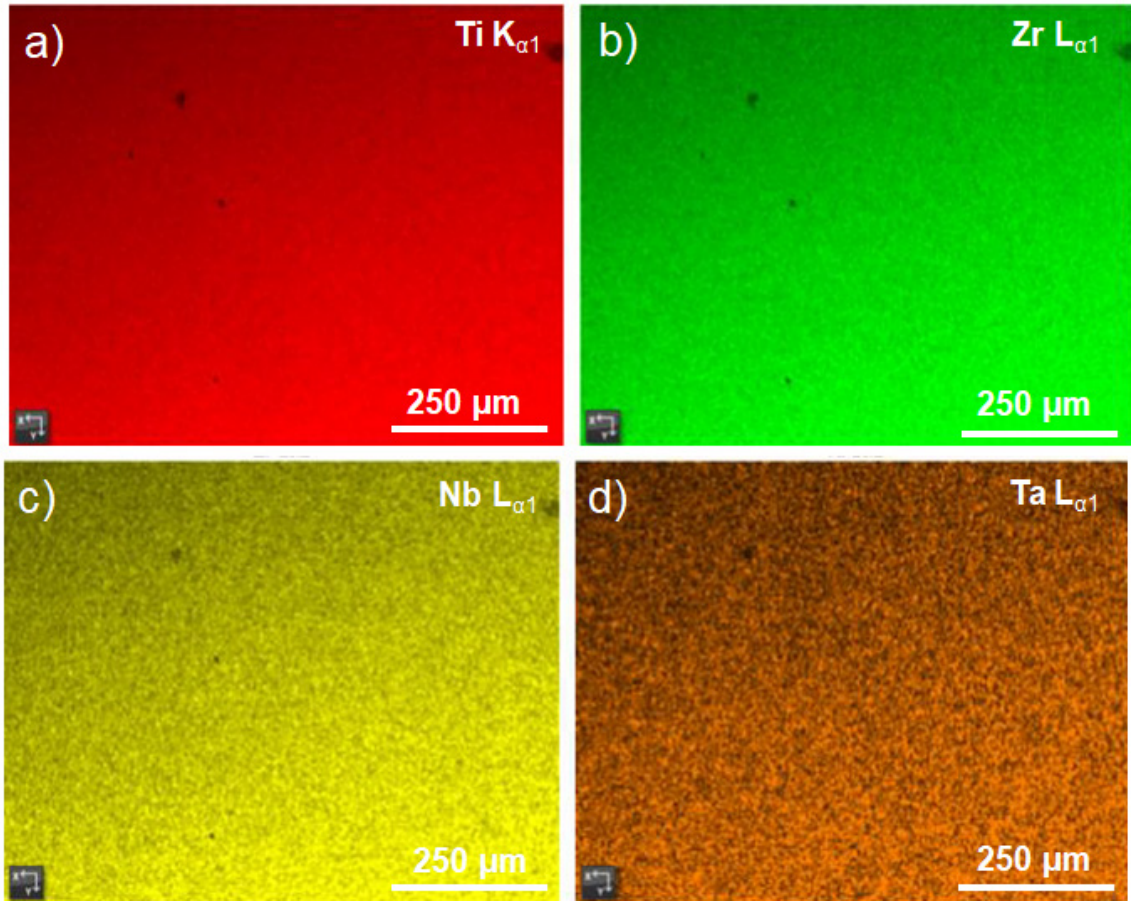

Figure 3. Map distribution of the Ti (**a**), Nb (**b**), Zr (**c**), and Ta (**d**) elements of the as-cast TNZT alloy.

In order to study grain size, morphology and crystalline orientation, the as-cast TNZT's microstructure was further investigated by the EBSD. The inverse pole figures corresponding to stereographic planes (001), (101) and (111) showed that grains were more randomly oriented and lacked a crystallographic texture (Figure 4). As in the XRD patterns, a β-Ti phase was indexed in the EBSD, which is related to the small volume fraction and grain size of the α″ martensitic laths. The crystallographic grain size of the β phases was determined by the EBSD experiments. The ECD value was 285.62 ± 199.51 µm, with minimum and maximum ECD values of 50.46 and 999.36 µm, respectively, in relation to the equiaxial grain morphology structure present in a larger quantity of as-cast TNZT. Some elongated grains were also identified. Orientation misfits had low-angle grain boundaries (LAGBs) of approximately 16.2% with angles within the 2–10° range, high-angle grain boundaries (HAGBs) of approximately 83% and angles of >10°. It is known that atoms are linked less regularly along grain boundaries and, therefore, interfacial energy is in accordance with the degree of disorientation, which is higher for HAGBs. Chemically speaking, boundaries are more reactive than grains with higher energy. When cells and fluids come into contact with these regions, they are expected to display different responses compared to the alloys formed mainly by LAGBs and to have larger grain sizes. Total interfacial energy is generally lower in materials with bigger grains given the smaller total contour area in these materials, and the bimodal grain size area distribution of the as-cast TNZT samples. A minimum area grain size of 20/100 µm^2 and a maximum one of 7844/100 µm^2 were found, with a final area of an average grain size of 945/100 µm^2. In this way, both grain size and HAGBs are related to corrosion and biological properties.

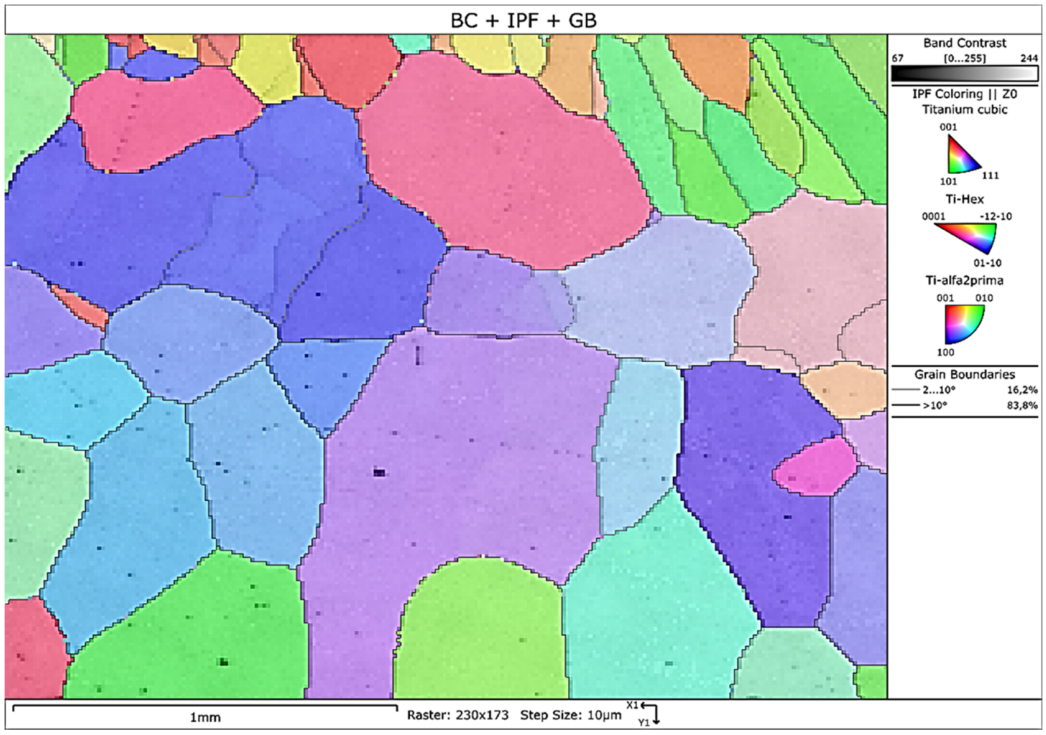

Figure 4. The EBSD analysis of as-cast TNZT with the inverse pole figure referring to the Ti cubic structure.

No α-Ti content was detected, and low α″-Ti content (martensitic structure) was located on the β-Ti grain boundaries, as indicated in Figure 5 in yellow color. This last phase presented small needles morphology, which the XRD pattern was capable of detecting, despite the low content.

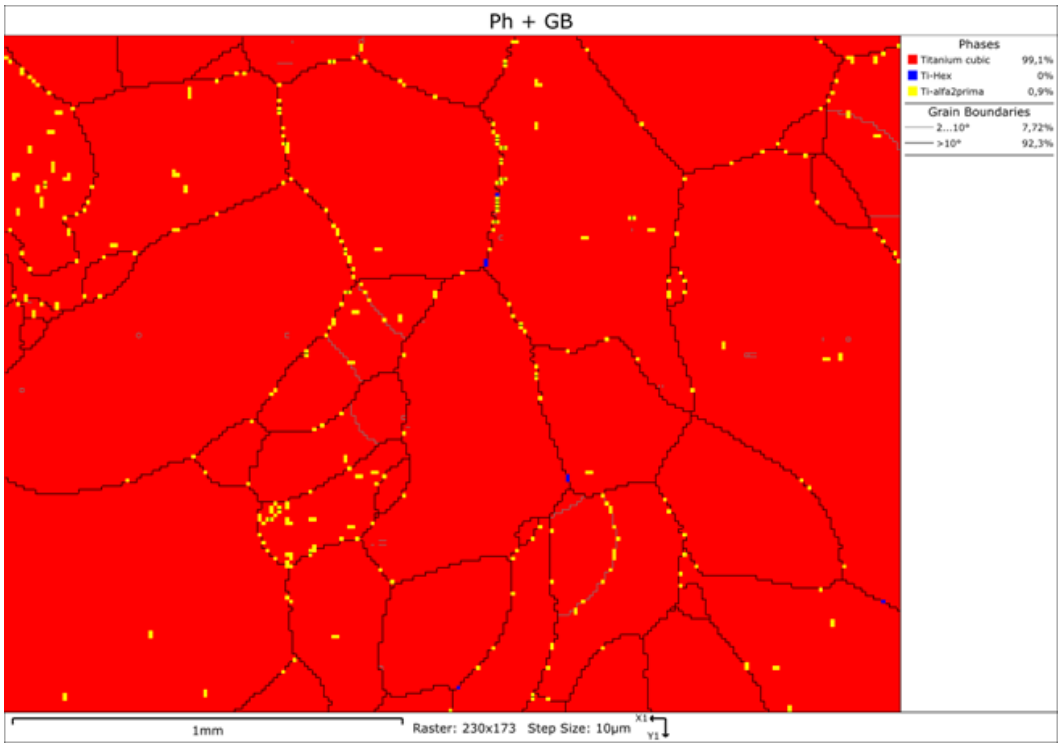

Figure 5. Phase-contrast image by EBSD analysis of as-cast TNZT.

According to these two microstructural characterization tests, the predominant phase in this alloy was the β phase because it constituted more than 90%. Nb and Ta were stabilizing β elements and, although Zr was considered a neutral element in the binary Ti alloys, it was also taken as a β stabilizer element when it formed part of the Ti alloys containing Nb and/or Ta [5].

Thus, the bcc structure was the predominant structure in this alloy. It was a more ductile alloy compared to the Ti-6Al-4V alloy, which had Al and, therefore, a higher percentage of α stabilizer with an hcp structure. This structure also led to an elastic modulus close to that of bone. This guarantees β-Ti alloys like TNZT are excellent for promoting a bone-implant interface that does not compromise load shielding and, therefore, their failure percentage is low [19].

3.2. Mechanical Properties Characterization

The representative stress–strain curves obtained from the full-scale 4-point bending test for as-cast TNZT, CP-Ti and Ti-6Al-4V were plotted and are represented in Figure 6a–c. The bending stress–strain curve of as-cast TNZT (Figure 6a) exhibited reasonably large total amounts of strains compared to Ti-6Al-4V and CP-Ti (Figure 6b,c). The elastic strain was ~0.016 mm, similarly to 0.016 and 0.015 mm of CP-Ti and Ti-6Al-4V, respectively. As the elastic strain was present in all the samples, strain hardening took place and the UTS value for as-cast TNZT was approximately 735 MPa, higher than 605 MPa for CP-Ti and lower than 1934 MPa for Ti-6Al-4V. Once the samples had reached UTS, the necking zone was reached for CP-Ti and Ti-6Al-4V, where plastic deformation still occurred and concentrated on the neck to the point at which the material broke. Both materials were checked for the region preceding fracture, except for one as-cast TNZT sample. Besides, compared to the reference samples, the stress–strain curve of the as-cast TNZT, is distinguished by the embrittlement that occurs in the final of the curve (approximately 700 MPa). Even with the low hardness presented in the as-cast TNZT, this final fracture should be related to the possible hydrogenation of the metals. In the α + β alloys, when a significant amount of β phase is present, hydrogen can be preferentially transported within the β lattice and can be reacted with the α phase along the α/β grain boundaries. Under these conditions, degradation will generally be more severe with the severity of degradation reflecting the hydrogen pressure dependence of hydrogen transport within the β phase [20]. In a Ti-6Al-4V alloy, thermomechanically treated in two distinguished microstructures, duplex and fully-lamellar, as described by Gutelmacher & Eliezer [21], hydrogen content measurements after high [4] and low fugacity hydrogen charging [21], revealed that the hydrogen concentrations absorbed in the fully-lamellar alloy are always higher than in the duplex microstructure, irrespective of the charging conditions. Since the rate of hydrogen diffusion is higher by several orders of magnitude in the β phase than in the α phase [22], microstructures with a more continuous β phase, such as fully-lamellar microstructure, will absorb more hydrogen than those with discontinuous β, such as the fine equiaxed α in the duplex microstructure, which corroborates with ours results in Figures 5 and 6. In more detail, for metals in the group IV transition metals, hydrogen tends to occupy tetrahedral interstitial sites' [23] higher solubility, as well as the rapid diffusion (especially at elevated temperatures) of hydrogen produced in the β-Ti. The presence of hydrogen in solid solution in both α and β phases resulted in lattice expansions which means that the β-Ti alloys do not tend to form hydrides due to their high hydrogen solubility and usually, especially at room temperature and low hydrogen pressures, they are considered to be fairly resistant to hydrogen embrittlement. However, some authors have demonstrated that β- Ti alloys can be severely degraded on exposure to hydrogen in different ways. The most evident way of degradation is by the formation of brittle hydride phases, similar to the degradation of primarily α alloys, except that it requires higher hydrogen pressures [24]. In addition, it has been observed that hydrogen in solid solution in the β lattice, well below the expected terminal solubility limit for the formation of a hydride, can have a significant effect on the ductile-to-brittle fraction transition of the β alloys. Besides, some

studies have been demonstrated that in terms of mechanical behavior, precipitation of metastable phases like ω phase in Ti alloys is not desirable, since it may lead to excessive embrittlement, loss of ductility and fatigue resistance, and must therefore be avoided [25], which also corroborates with our results, as seen in Figures 2 and 5. The E_B calculated from the bending strength data was 43 GPa for as-cast TNZT, which can be compared to the literature (tensile properties) on 55 GPa [26]. This means that it came closer to the trabecular and cortical bone than CP-Ti and Ti-6Al-4V (seen in Figure 6d). Moreso, σ_B was calculated according to Equation (5), and the obtained values appear in Table 2. The value for as-cast TNZT was similar to that for CP-Ti and lower than that for Ti-6Al-4V. These data confirmed that the TNZT alloy offered good flexural behavior, a closer elastic modulus to bone tissue, and lower hardness than CP-Ti and Ti-6Al-4V. In the field of implants for dentistry applications, hardness for dentin is 53–63 HV and 283–374 for enamel [27]. Its yield stress is 523 MPa in the event of bending. It was 687.03 MPa compared to the Ti-Nb-Zr alloy (without Ta), which came very close to that of 680 MPa for Ti-6Al-4V [6]. These mechanical characteristics are related to these materials' microstructure. Both CP-Ti and Ti-6Al-4V had a considerable σ phase compared to TNZT, where the β phase predominated. The bcc crystalline structures (β phase) presented less deformation resistance compared to the hcp structures (α phase), which was in accordance with the decreased hardness in the β-type alloys, in addition to lesser interstitial solid solution strengthening in the β phase. It makes sense that a lower force would be necessary to enter the section where deformations were not transitory (area beyond the yield stress). For to be sure about the safe material in the bio-environment, it is necessary to evaluate the fatigue properties of the material and understand the implant failure mechanism from fatigue crack propagation.

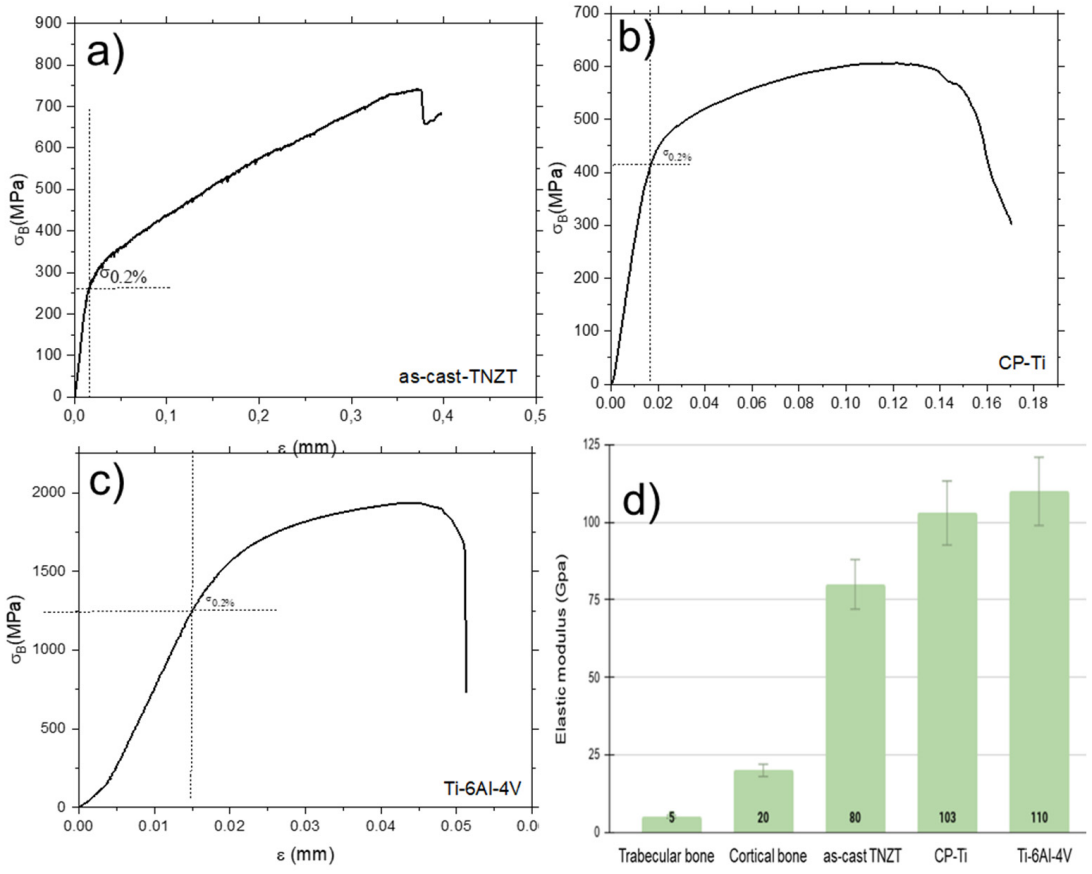

Figure 6. Bending stress–strain curves of as-cast TNZT (**a**), CP-Ti (**b**) and Ti-6Al-4V (**c**). A comparison of the elastic modulus to them and to bone (**d**) comparison of elastic modulus of as-cast with CP-Ti, Ti-6Al-4V and bone tissue, obtained by ultrasound.

Table 2. Mechanical parameters obtained from the flexural strength tests and hardness.

Materials	Yield Strength (MPa)	ε_B (%)	E_B (GPa)	Hardness (HV)
TNZT	200 ± 24	38 ± 1	43 ± 5	94 ± 4
CP-Ti	377 ± 17	18 ± 4	79 ± 23	241 ± 7
Ti-6Al-4V-ELI	1594 ± 64	6 ± 1	111 ± 14	172 ± 19

The elastic modulus obtained by ultrasound had a value of approximately 80 GPa, which was 20–25% lower than that of other available alloys [28]. In the literature, some authors have described different elastic modulus values in distinct tooth kinds; e.g., for incisors, premolars and third molars, and elastic moduli ranges in enamel are, respectively, 98.3, 40–80 and 75–90 GPa. The same samples had values of 24.8 GPa, 60–100 GPa in dentin [28–30] and no value description for the third molar was found. As previously analyzed, this reduction in elastic modulus denotes a marked change in the transmission of masticatory loads (for dental implants) between bone and the implant. As previously explained, the yield stress of TNZT was slightly lower (without being compromised) than the other employed alloys, and this decrease led, in turn, to a lower Young's modulus. The combination of both factors highlights this alloy from many others.

3.3. Chemical and Electrochemical Characterization

The as-cast TNZT ions were studied in the modified Ringer-Hartmann electrolyte. The metal ions released in these tests were identified as a cause of cytotoxicity effects, as discussed later.

The results of the modified Ringer-Hartmann artificial saliva, together with the ions released from the as-cast TNTZ in it, were used to study the cytotoxicity that came into contact with hDPSCs and MG-63. The data showed that the concentration of the Ti ions released by the Ti-6Al-4V alloy was notably higher than that by CP-Ti and as-cast TNZT (Figure 7). The release of Al and V, compared to Nb, Zr and Ta, gave a high release concentration. All ions in significant amounts are toxic, but some are more tolerated by the human body than others. Al causes cognitive decline in the people exposed to it, while Alzheimer's disease and other neurodegenerative disorders have been related to Ti exposure. Al has even been proposed as an etiology [31]. These data warn and encourage us to continue investigating TNZT alloys for the biocompatibility and low ion release concentration that their elements present. Thus, it can be stated that the order of resistance to the surface etches of the samples in contact with the modified Ringer-Hartmann solution for 30 days was as-cast TNZT > CP-Ti > Ti-6Al-4V. These differences are due to the chemical composition and microstructure making up the studied different materials. Metallic ions are easily released from the microstructure with smaller grains, and this was achieved in line with the followed processing. Another point is that the quicker passivation, the stronger the oxide films that form on the surface of Ti materials, given their high reactivity. Furthermore, greater corrosion resistance appears in materials with a higher grain fraction, which leads to a stable oxide layer. As discussed before, grain boundaries have higher energy and are, therefore, more reactive than grains. Thus, producing a rapid formation of passive films and impurity segregation on their surfaces makes sense. However, as the as-cast TNZT alloy is formed by more than 90% of the β phase, its grain boundaries are structured mainly with HAGBs with an ECD value of 285.62 ± 199.51 μm, which agrees with our results. In this way, the total interfacial energy is lower in the materials with larger grains as the total contour area is smaller in these materials. The CP-Ti grain size was 11.56 ± 5.83 μm. Ti-6Al-4V was formed with 1.45 ± 0.13 μm for the α phase and 0.74 ± 0.02 μm for the β phase. Another point that can help to make as-cast TNZT more resistant, is biocorrosion, due to the presence of Nb and Zr, which exhibit ideal passivity and are not prone to the passive layer's chemical breakdown by exhibiting minimum passive dissolution rates. In fact, Nb and Zr contribute to the formation of a spontaneous highly protective passive film on Ti alloys and, unlike Al and V, are not released into the

environment as dissolved metal ions. Moreover, smaller ions are more easily released. Al (0.143 nm) and V (0.132 nm) had smaller atomic radii than Zr (0.159) and Ta (0.149).

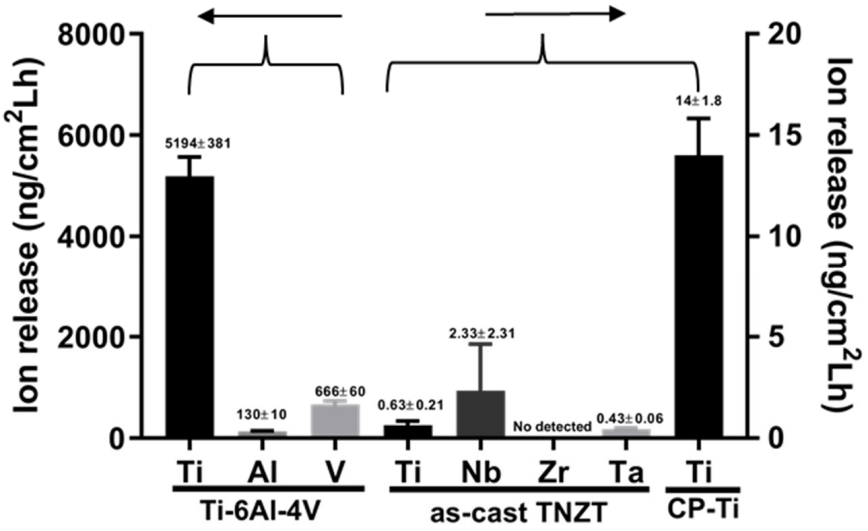

Figure 7. Concentrations of the ions released for CP-Ti and Ti-6Al-4V compared to as-cast TNZT after 735 h of immersion.

Open-circuit potential (OCP) measurements were taken on as-cast TNZT, and CP-Ti and Ti-6Al-4V were used as controls. The representation of OCP versus time is seen in Figure 8a, where the OCP of as-TNZT is lower than the controls but is constant and related to the passive layer formed between 0.1 and 0.6 h to reach −0.410 V. CP-Ti and Ti-6Al-4V differed by presenting a more cathodic potential and kept increasing to 0.6 h to delay passive layer formation. To analyze the active and passive regions, as well as the cathodic-anodic transition point, potentiodynamic curves (PPCs) were studied. They are indicated in Figure 8b. Samples exhibited similar polarization behaviors, which can be seen in the anodic zone for three samples whose potential corrosions are −0.503 V for as-cast TNZT, −0.280 V for CP-Ti and 0.282 V for Ti-6Al4V. For as-cast TNZT in Figure 8a, it is possible to note that the sample reaches faster the corrosion potential in more negative potential, which means it will be more stable compared to CP-Ti and Ti-6Al-4V. The i_{corr} of as-cast TNZT presents the same magnitude of CP-Ti and is higher than Ti-6Al-4V, indicating that the dissolution of as-cast TNZT occurs faster than Ti-6Al4V. As the dissolution mechanism is proportional to the i_{corr}, in a more negative current density, higher is the dissolution of the material.

Pitting corrosion could not easily happen for CP-Ti and the as-cast TNZT alloy because it could simultaneously introduce metals with plenty of dislocations in grain interiors and boundaries. Passive film nucleation could form in grain interiors and boundaries at the same time, which would make passive films denser to resist aggressive ion penetration to present higher current densities. The passive current density of Ti-6Al-4V was much lower than the others, which indicates that the passivation film would be more prone to self-repair after pitting corrosion. This is attributed mainly to high storage energy in the dislocations and grain boundaries in Ti-6Al-4V, which is beneficial for passivation film formation and, thus, enhances this film's self-repair ability. In the work of Garcia-Ramirez et al., 2018, the samples made with Ti-Ni-Al with different chemical compositions produced several kinds of grains and sizes [32]. Corrosion resistance was greater for those with a big grain size, which corroborates our results. Although the rate of corrosion for as-cast TNZT was close to the Ti-6Al-4V and higher compared to CP-Ti (Table 3), it can be concluded inferior corrosion properties compared to reference materials used in this work do not occur in the ion release. The mechanism of corrosion between the ion release and the potentiodynamic are distinct. The first one represents the corrosion at a more natural level, which simulates the body

conditions. The samples were immersed in bottles with fluid with pH and similar saline compositions and temperature for 735 h. According to the theory of passivity, metallic biomaterials in aqueous solutions are systems in which active and passive surfaces exist simultaneously in contact with electrolytes [33]. Therefore, it is now thought that the surface oxide film on the materials repeats a process of partial dissolution and reprecipitation in an aqueous solution. If the dissolution rate is larger than the reprecipitation rate, metal ions are gradually released. This process is "anodic dissolution" [34]. If the potential of a material anodically changes, then the anodic dissolution rate increases. The metal ion release remaining on the surface oxide film is relatively slow in vivo because the change in potential of the material in vivo is usually small.

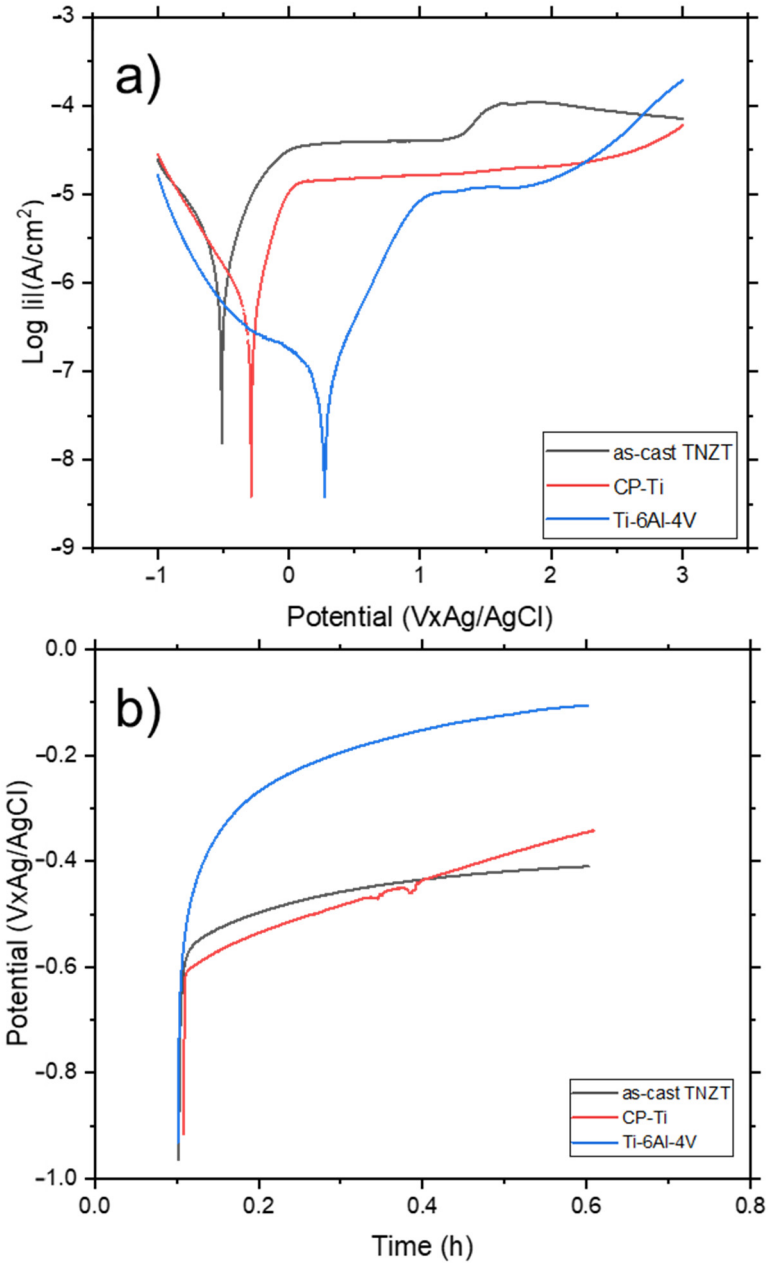

Figure 8. Representation of the OCP (**a**) and PPCs (**b**) curves of two cast TNZT alloy samples. The measurements were carried out in Ringer-Hartmann solution (pH = 6.8) at 37 °C.

Table 3. Kinetic parameters obtained by the polarization curves (PPCs) in Figure 8. First, an average of the parameters of the three curves was made and the final result can be found in this table. The R_p values were obtained by Equation (3).

Materials	I_{corr} (A/cm^2)	E_{corr} (V)	R_p (kΩ.cm^2)	C_r (μm/Year)
As-cast TNZT	$5.94 \times 10^{-7} \pm 1.98 \times 10^{-7}$	-0.49 ± 0.03	45 ± 15.05	4.03×10^{-6}
CP-Ti	$5.37 \times 10^{-8} \pm 2.10 \times 10^{-8}$	-0.25 ± 0.13	509 ± 199	4.59×10^{-7}
Ti-6Al-4V	$1.47 \times 10^{-7} \pm 1.03 \times 10^{-7}$	-0.18 ± 0.02	231 ± 129	1.25×10^{-6}

Even though the potentiodynamic assay was carried out at the same temperature, using the same saline solution, a current passes between a metal sample of interest and an inert electrode in a given solution to alter the electrochemical potential (V) of the test sample allows for the systematic characterization of the material by determining the breakdown potential. This is to further understand the material's response to corrosion, being more aggressive than the ion release assay, which explains the significant difference found in the as-cast TNZT samples.

It is known that an ideal bone implant should progressively degrade at a suitable rate (approximately 0.2~0.5 mm/year) to match the bone healing process, which demonstrates good resistance of as-cast TNZT in the biological simulated fluid.

3.4. In Vitro Biological Properties of As-Cast TNZT

3.4.1. Artificial Saliva

First, cytotoxicity was measured using the hDPSCs and MG-63 cells treated with increasing concentrations of pure artificial saliva (modified Ringer-Hartmann solution) mixed with culture medium (0.05%, 0.1%, 0.5%, 1%, 2%, 5%, 10%, 25% and 50%). Figure 9 shows that all the pure artificial saliva concentrations, except the last one (50%), had no significant effects on the cell viability of both cells hDPSCs and MG-63. Viability was close to C- and very close to 100%. In this way, concentrations of up to 25% were used for the next steps and the biological studies.

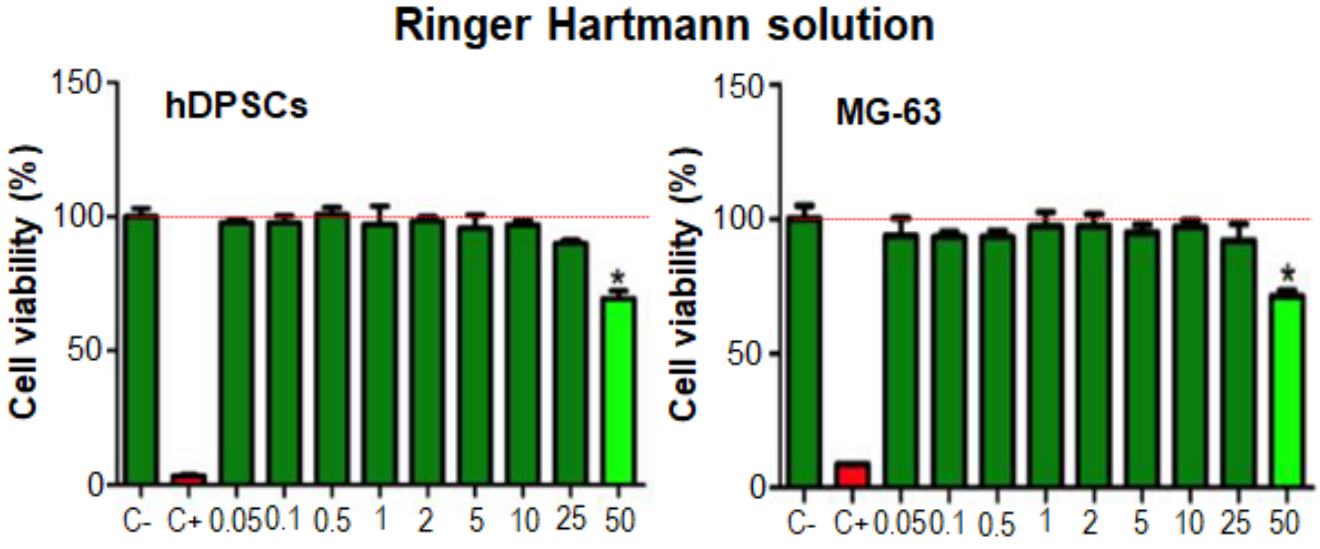

Figure 9. Measurement of the cytotoxicity of Ringer-Hartmann's solution in cells hDPSCs and MG-63 at different concentrations. * when is $p < 0.05$.

Cytotoxicity testing was carried out on the three different alloys (CP-Ti, Ti-6Al-4V, TNZT) as seen in Figure 10. The software employed for the analysis of the results (GraphPad Prism 7.3) allowed the normalization of all the results from the different tested plates. The control was set at 100% cell viability. The negative control (C-) corresponded to cells

hDPSCs and MG-63 cultured with their proliferation medium. In this way, it was possible to compare all the obtained results to the other tested alloy types. The measurements taken of the other wells were also compared to this control, and it was analyzed whether or not there were significant differences between them and the control (*) using the post hoc Tukey test by multiple comparisons. Thus, in those cases with a significant result, a certain degree of cytotoxicity of the ions released by the alloy in question was concluded. Although the modified Ringer-Hartmann (Ps) artificial saliva did not generate any toxic effect, it was tested on each plate to make sure. Latex was employed as a positive control (C+), which was always significant compared to the negative control because it caused cell death. Next, the behavior of the samples corresponding to artificial saliva with the ions released from different alloys (M) was analyzed. Cells hDPSCs in the presence of modified Ringer-Hartmann artificial saliva with released ions showed optimal cell viability in the commercial pure Ti manufactured by forging. These results were used as a control to analyze the influence of the other elements added to Ti in the other alloys. According to Kuroda et al., 1998, cytotoxicity of Al and Va metallic ions was detected in biomedical alloys [3]. Al was the ion released in the most artificial saliva compared to others. The obtained results were similar because it was the same alloy. The cell viability percentages for the three sample contents allowed us to conclude that there was no evidence of the Ti-6Al-4V alloy being cytotoxic for human dental pulp stem cells. The results enabled us to verify that, in the artificial saliva with the ions released from as-TNZT, once again, cells showed cell viability in line with that of those cells in their own proliferation medium. Thus, for cells hDPSCs, it was concluded that none of the three alloys presented relative differences to the control. This study allowed us to affirm that the incorporation of Nb, Zr and Ta into Ti to form the quaternary alloy as-cast TNZT was also positive in cell viability terms. The same analysis was carried out below, but with the MG-63 cell line, to define these alloys' behavior when they came into contact with similar cells to osteoblasts. The study of these cells' behavior before the ions were released from the alloys in artificial saliva is most important because, once the dental implant is placed in a patient, the aim is for part of the stem cells of the human dental pulp to differentiate into osteoblasts to promote the implant's osseointegration with the surrounding bone. First, the alloy generated in the laboratory showed increased proliferation in proportion to the present sample's increase. It was concluded that this alloy promoted MG-63 cell line growth. The behavior of the pure Ti obtained by forging was the exact opposite. It was maintained at the same levels as the control for the 1% sample but, as the percentage of artificial saliva introduced into dilution rose, cell viability was considerably reduced by 30%. A trend was generated, which allowed us to predict that cells would die as the artificial saliva dissolution with the released Ti ions increased. This is, hence, an indication of the cytotoxicity of this specific CP-Ti sample for MG-63 cells.

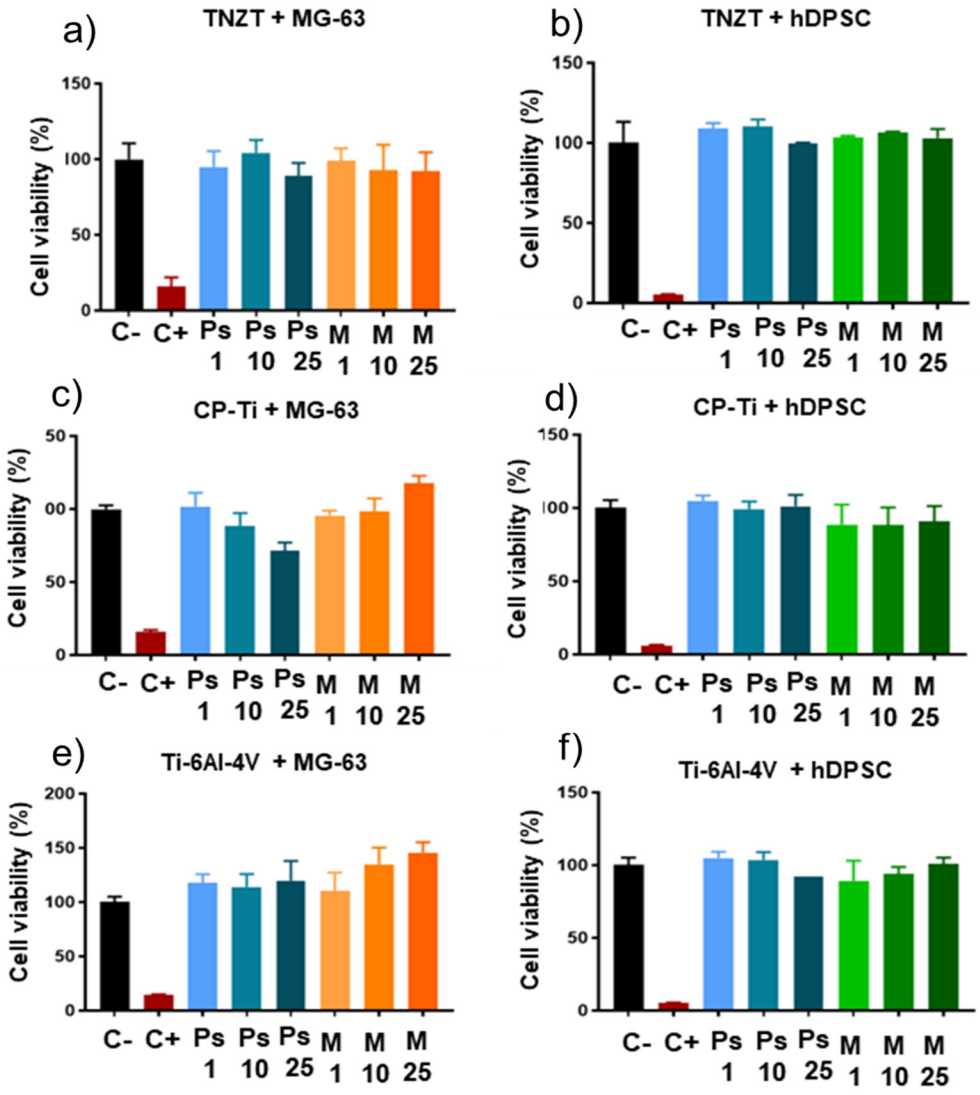

Figure 10. Cell viability of cells hDPSCs and MG-63 cells when they came into contact with different pure saliva (PS) concentrations, and also with the different concentrations of the ion released solutions containing possible ions related to as-cast TNZT, CP-Ti and Ti-6Al-4V. (**a**) Cell viability of as-cast Ti-Nb-Zr-Ta in contact with MG-63. (**b**) Cell viability of as-cast Ti-Nb-Zr-Ta in contact with hDPSCs. (**c**) Cell viability of CP-Ti in contact with MG-63. (**d**) Cell viability of CP-Ti in contact with hDPSCs (**e**) Cell viability of Ti-6Al-4V in contact with MG-63. (**f**) Cell viability of as-cast Ti-6Al-4V in contact with hDPSCs.

3.4.2. Osteocalcin Expression and F-Actin Staining in Cells hDPSCs and MG-63 in Contact with As-Cast TNZT

Another factor that also helped to confirm this differentiation was to study cell morphology. Cells hDPSCs in their proliferation medium showed their own F-actin. However, the morphology of these same cells cultured during the experiments with differentiation modified medium presented F-actin of different sizes and shapes and was narrower than with the proliferation medium. The cells in 2D culture proliferated and differentiated. This behavior was also expected, and optimal and relevant results were obtained by in vitro experimentation with as-cast TNZT. The adhesion and survival of two cell lines on the 3D samples were demonstrated in both the analyzed media.

A dental implant is an external prosthesis that is introduced into patients and can be accepted or rejected depending on the patient's response. The importance of the human body accepting dental implants lies, to a great extent, in the interface between the implant

and bone. If it promotes the regeneration of the area by differentiating the surrounding cells into different cell types, such as osteoblasts, the implant's success rate increases. To date, no studies have focused on cell differentiation in contact with as-cast TNZT alloys. As proven in the biological tests carried out in this work, the as-cast TNZT alloy managed to achieve this osteo-differentiation with considerable cell adhesion, survival and differentiation. It did not produce cytotoxicity, and the cell viability values came very close to those of the control group. These tests prove the biocompatibility of the TNZT alloy as a material to form biomedical prostheses.

After 4 weeks in culture, F-actin distribution was evaluated by fluorescent staining with the phalloidin-rhodamine conjugate to define both cell morphology and osteocalcin (OC) using immunofluorescence to confirm the possible differentiation of hDPSCs cells to osteoblasts, where MG-63 was always employed as the control. A search was made on the surfaces of wells and disks to find any areas with only a few cells, as shown in the following figure, to analyze their morphological properties and the possible presence of OC in more detail.

Figure 11 shows the OC expression visualized in green for the hDSPCs and MG-63 cells treated with conventional medium (Figure 11a,b) and differentiation medium (Figure 11c,d) on a flat surface (2D). The nucleus was stained with DAPI (blue) to better identify any cells present. The greater cell proliferation of MG-63 than hDPSCs was initially noted, and OC with a low intensity was detected only in cells MG-63. In the hDPSCs cells with the differentiation medium, a change was noted in the nucleus morphology, which is a clue to indicate that the differentiation process had started.

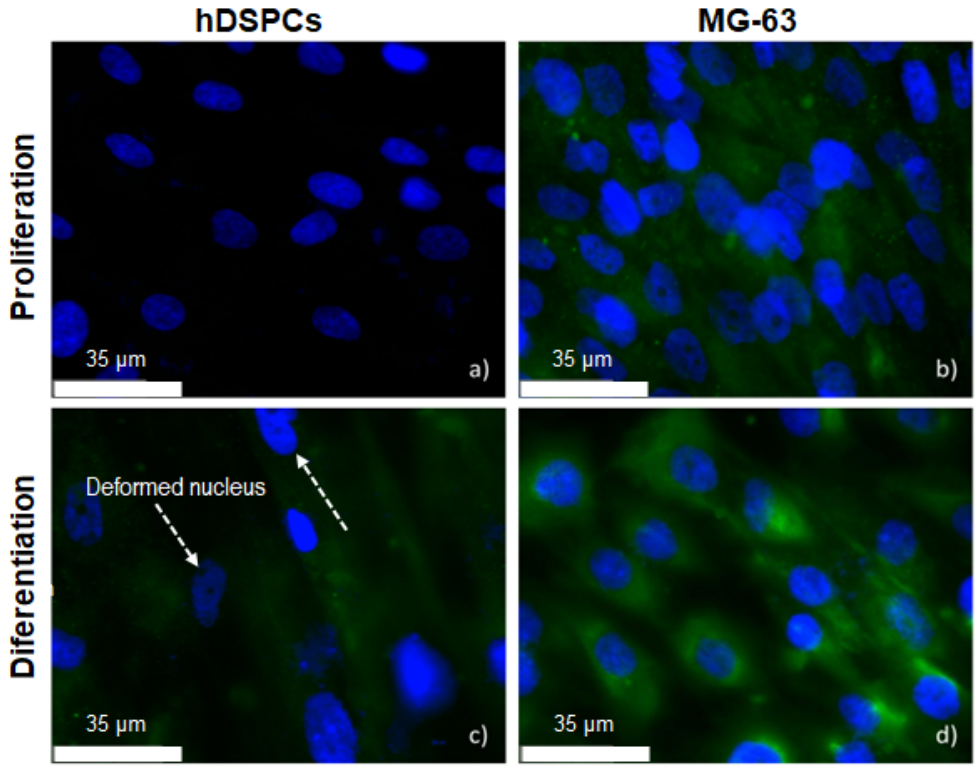

Figure 11. Immunocytochemical staining with osteocalcin (OC) and counterstained with DAPI in the hDPSCs and MG-63 cells cultured in conventional medium (first line) and differentiation medium (second line) on flat surfaces (2D). (**a**) Immunocytochemical staining of hDPSCs in conventional culture medium. (**b**) Immunocytochemical staining of MG-63 in conventional culture medium. (**c**) Immunocytochemical staining of hDPSCs in differentiation culture medium. (**d**) Immunocytochemical staining of MG-63 in differentiation culture medium.

When switching to a 3D culture system (over the as-cast TNZT alloy's surface), the number of proliferating cells grew under all four conditions compared to 2D plating (Figure 12a–d). As shown in Figure 12a–d, the presence of OC was not detected in hDPSCs when subjected to a conventional culture medium. MG-63 displayed a mild OC expression, but with less homogeneous spatial distribution (Figure 12b). By adding the differentiation medium, the number of proliferated cells dropped and followed the same trend as shown in Figure 13, with a lower OC expression compared to MG-63. Nucleus morphology changes were seen for both cells (Figure 12c,d).

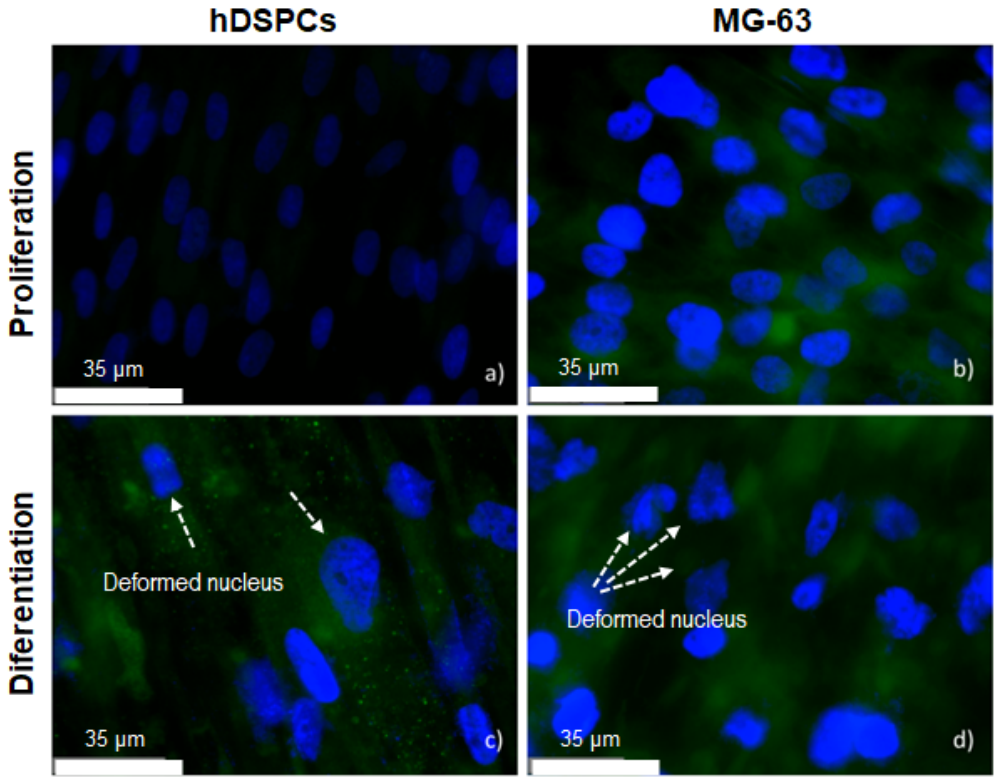

Figure 12. Immunocytochemical staining for osteocalcin counterstained with DAPI in the hDPSCs and MG-63 cells cultured in conventional medium (first line) and differentiation medium (second line). They were all cultivated on as-cast TNZT surfaces (3D). (**a**) Immunocytochemical staining of hDPSCs in contact with the as-cast TNZT surface in conventional culture medium. (**b**) Immunocytochemical staining of MG-63 in contact with the as-cast TNZT surface in conventional culture medium. (**c**) Immunocytochemical staining of hDPSCs in contact with the as-cast TNZT surface in differentiation culture medium. (**d**) Immunocytochemical staining of MG-63 in contact with the as-cast TNZT surface in differentiation culture medium.

Figure 13a–d depicts cells hDPSCs and MG-63 when referring to the 2D plating of the images in Figure 11. Figure 13e–h refers to the hDPSCs and MG-63 with 3D plating and refers to Figure 12. All the figures present the mean of the green color intensity when referring to the OC expression obtained by histograms.

Finally, the comparisons of the green color intensities between the same cell type in platelets in both 2D and 3D are shown in Figure 14a,b. Figure 14c,d quantitatively confirms the increased OC expression in both cells when subjected to the differentiation medium. When evaluating the cellular behavior of cells MG-63, the expression significantly decreased in both the conventional culture and differentiation media. Furthermore, hDPSCs displayed the opposite behavior.

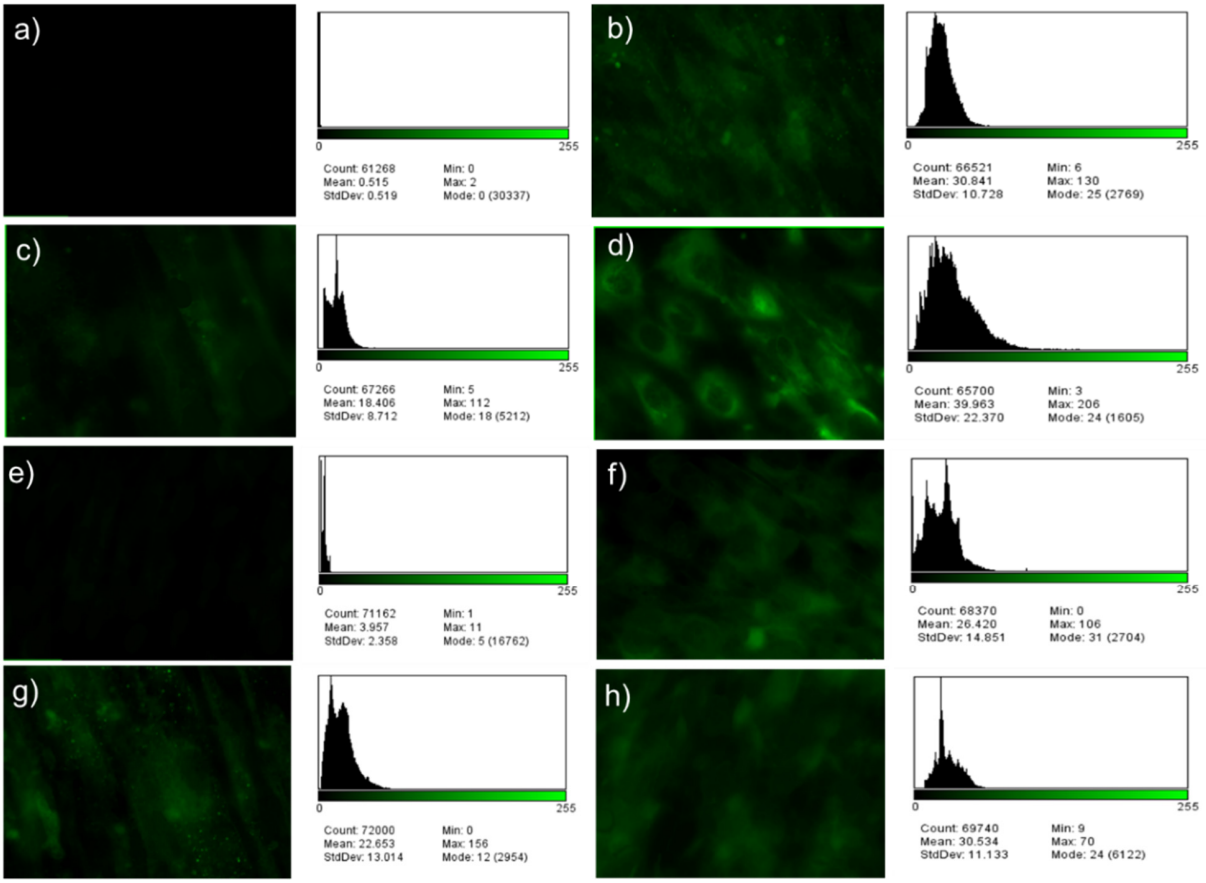

Figure 13. Fluorescence microscopic images and their analysis of histograms using the ImageJ software at 20×, (**a**–**d**) are the hDPSCs and MG-63 cells cultivated on flat surfaces in conventional and differentiation media in relation to Figure 11; (**e**–**h**) are the hDPSCs and MG-63 cells cultivated on as-cast TNZT surfaces in conventional and differentiation media in relation to Figure 12.

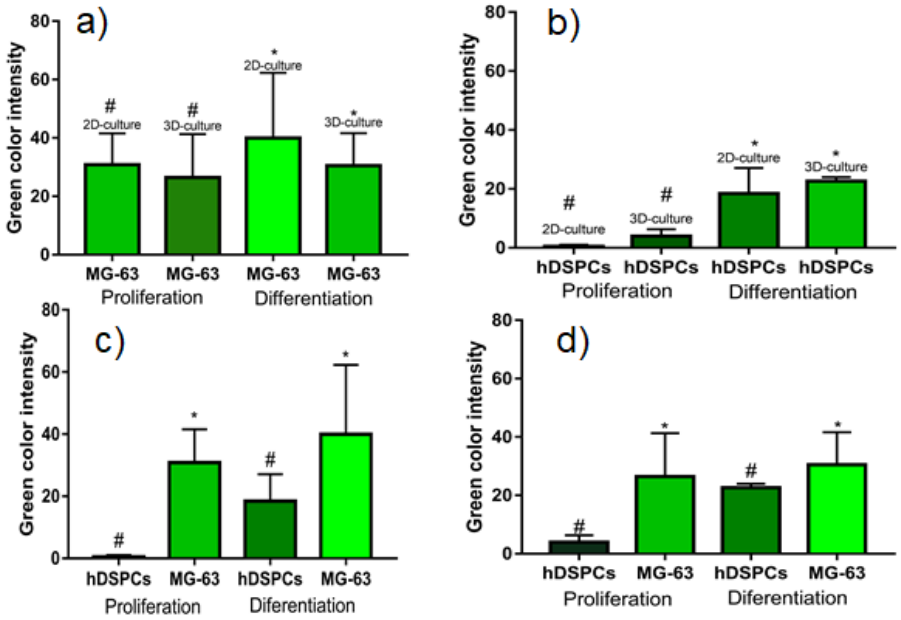

Figure 14. OCN expression with comparisons between the same cell line on 2D (**a**) and 3D (**b**) surfaces. OCN expression with comparisons between the same cell line (MG-63) (**c**) and (hDPSCs) (**d**) in different culture media # and * when $p < 0.05$.

F-actin (focal adhesion) staining was used to study the morphology structure of the hDPSCs and MG-63 cytoskeleton (Figure 15a–d) treated with conventional and differentiation culture media. The hDPSCs on flat surfaces showed a clear cytoskeleton and long "dash-like-" shaped focal adhesions, while cells MG-63 under some conditions displayed "dot-like" focal adhesions on the edge of the cells with no clear cytoskeleton structure.

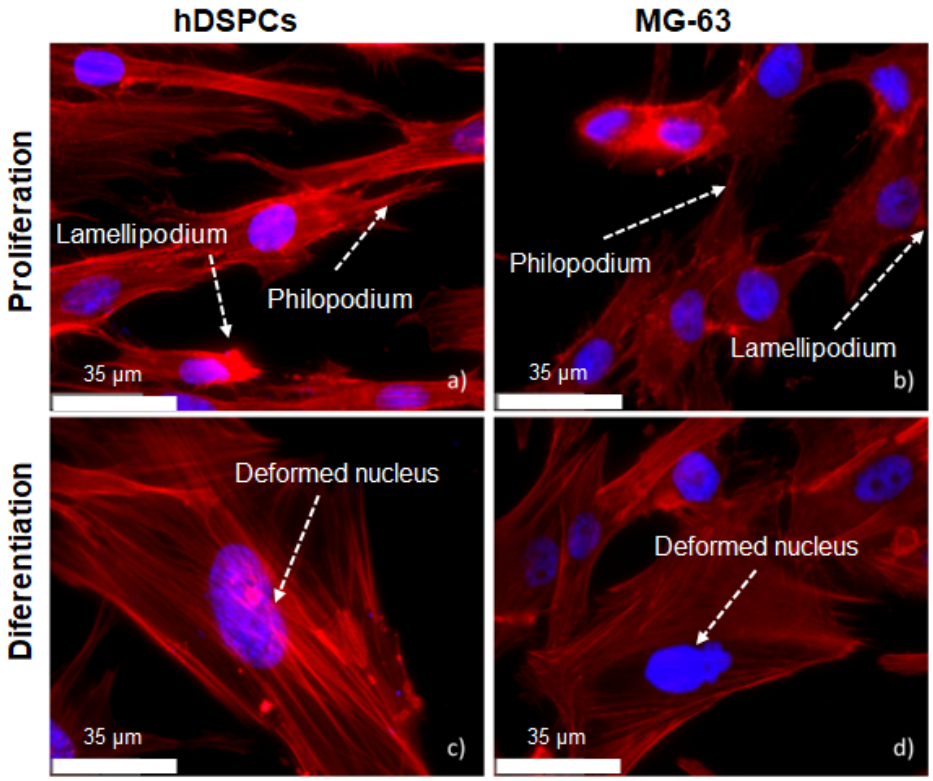

Figure 15. Immunocytochemical staining for F-actin (in red), and nuclei counterstained with DAPI in the hDPSCs and MG-63 cells cultured in conventional medium (first line) (**a**,**b**) and in differentiation medium (second line) (**c**,**d**). They were all cultivated on flat surfaces.

The cytoskeleton morphology was wider and more circular than in hDPSCs. In both cells line, cytoplasmic projections were seen, such as lamellipodium and philopodium, which are responsible for creating edges when treated with conventional and osteogenic culture media. Moreso, hDPSCs showed a clearer cytoskeleton and circular-shaped focal adhesions overlapping the cytoskeleton. The same morphology was found for cells MG-63 when treated with the osteogenic medium. Cell adhesion and, consequently, projections are fundamental for influencing nucleus deformation and, consequently, differentiation paths. When treated with osteogenic medium, both cells presented a deformed nucleus and a wider spread morphology on a flat surface.

Figure 16a–d represents cells hDPSCs and MG63 on the as-cast TNZT 3D surface. More proliferation is noted for cells when treated with conventional medium compared to the flat surface (Figure 15a,b). Furthermore, a typical clear cytoskeleton with long "dash-liked-" shaped focal adhesions (mature) overlapping the cytoskeleton can be seen. The more pronounced F-actin-containing focal adhesions were localized on cells' edges. MG-63 cells presented a circular cytoskeleton as they were widely spread on the 3D surface (Figure 16b), while the cytoplasmic projections responsible for cell–cell communication formed. The more pronounced F-actin localized on cells' edges is noted.

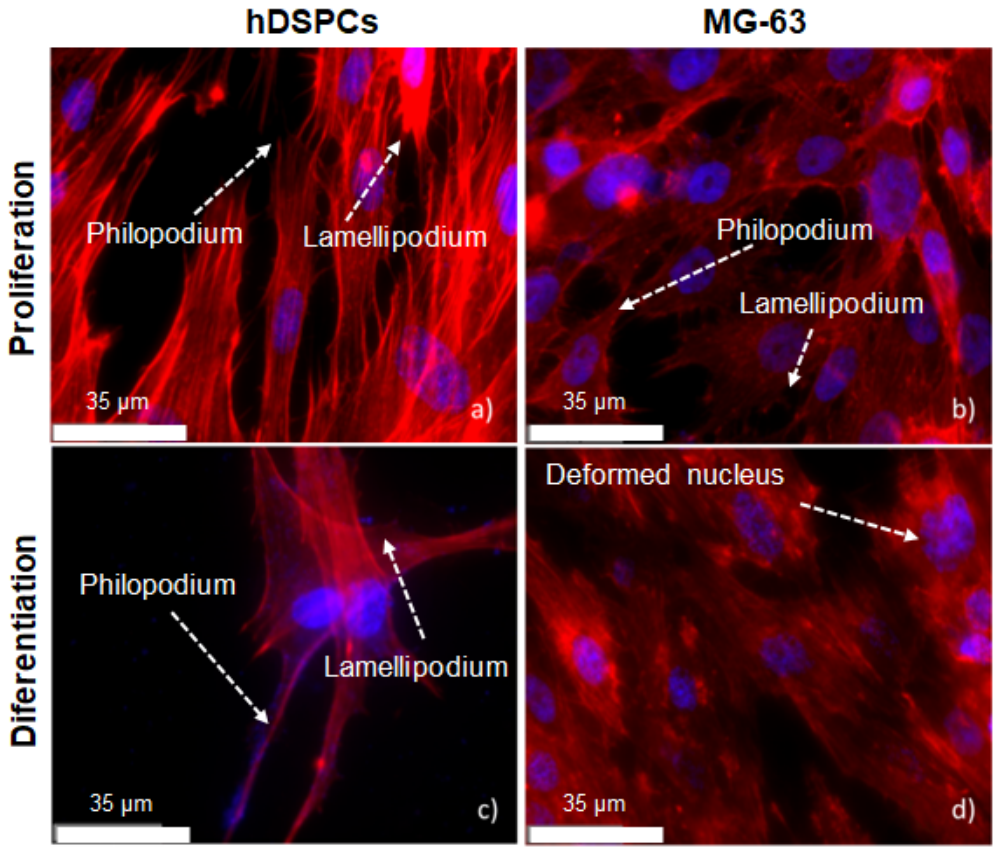

Figure 16. Immunocytochemical staining for F-actin (in red) and nuclei counterstained with DAPI in the hDPSCs and MG-63 cultured in conventional medium (first line) (**a**,**b**) and differentiation medium (second line) (**c**,**d**). They were all cultivated on as-cast TNZT surfaces.

Cells hDPSCs presented a small "dot-like" focal adhesion on cells' edges with pronounced cytoplasmatic projections responsible for cell-cell communication, while MG-63 on osteogenic differentiation medium showed a more circular cytoskeleton, with more pronounced F-actin focal adhesion on cells' edges (Figure 16c). Unlike hDPSCs, cells MG-63 did not present a well-organized and clear membrane, which suggests that the 3D microstructure surface significantly induced the osteogenic differentiation process (Figure 16d). Several studies have indicated that cell dispersion behavior associated with nucleus deformation plays a vital role in promoting cell mineralization and osteoconductivity.

In Figure 17a–d, images are shown together with the red color intensity histograms referring to the F-actin distribution, depicted in Figure 15. In Figure 17e–h, confocal microscopy images are indicated along with the histograms referring to the F-actin distribution of the images shown in Figure 16. From these results, no significant change in F-actin was observed in hDPSCs when subjected to osteogenic differentiation medium (Figures 17c,g and 18c,d), unlike MG-63, with increased cell adhesion, as indicated by the red color intensity referring to F-actin on both 2D and 3D surfaces (Figures 17b,d,f,h and 18a,c,d). However, the intensity was significantly greater for the hDPSCs treated with conventional culture medium on 3D surfaces (Figure 18b), and intensity significantly decreased for those submitted to differentiation medium. MG-63 displayed similar behavior to hDPSCs when treated with conventional medium (Figure 18a). The red color intensity of F-actin labeling significantly increased, as it did when treated with osteogenic differentiation means.

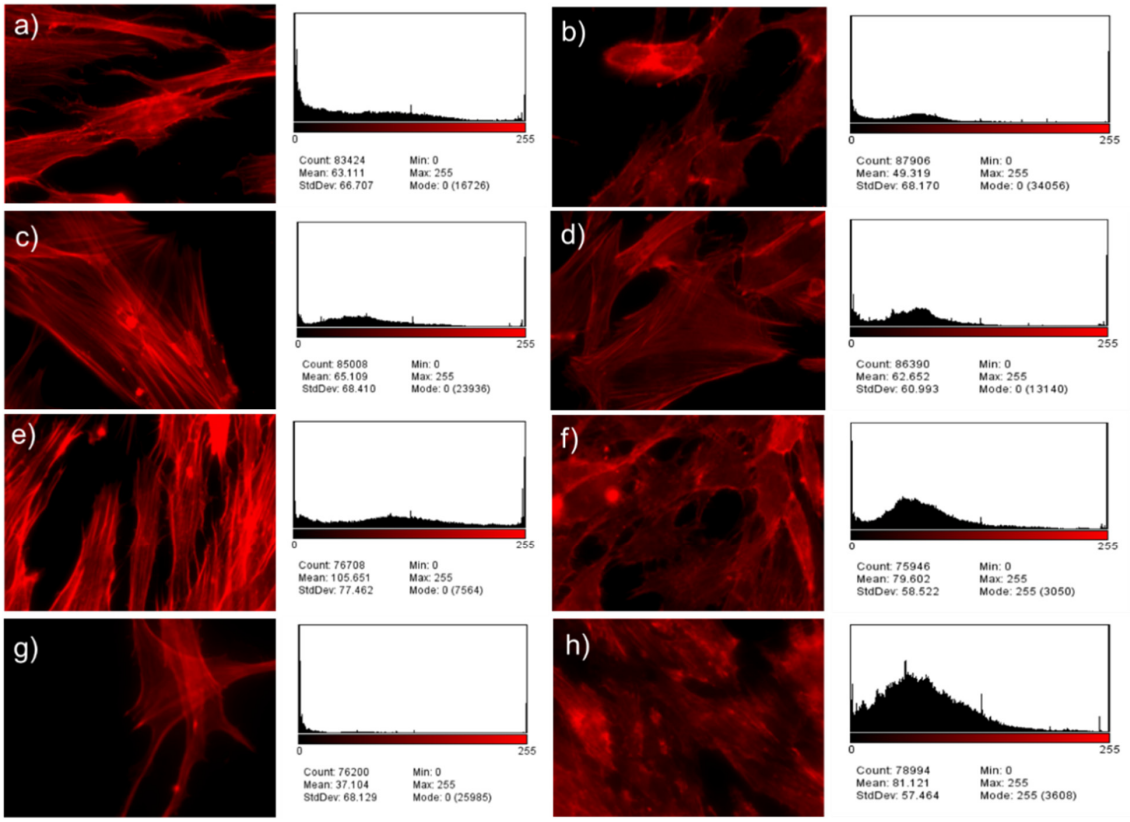

Figure 17. Fluorescence microscopic images stained for the cytoskeleton and their analysis with histograms employing the ImageJ software at 20×, (**a**–**d**) are the hDPSCs and MG-63 cells cultivated on flat surfaces in conventional and differentiation media in relation to Figure 15; (**e**–**h**) are the hDPSCs and MG-63 cells cultivated on as-cast TNZT surfaces in conventional and differentiation media in relation to Figure 16.

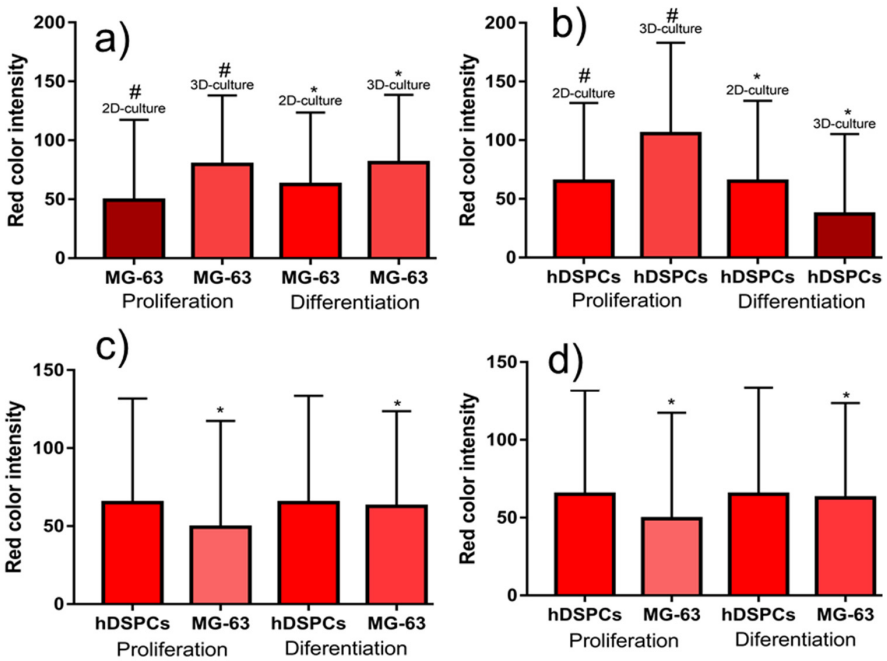

Figure 18. F-actin was quantified by the comparisons made between the same cell line on 2D (**a**) and 3D surfaces (**b**). F-actin intensity color was also used in the comparisons between the same cell line (MG-63) (**c**), (hDPSCs) (**d**). # and * when $p < 0.05$.

4. Conclusions

From the microstructure studies of the as-cast Ti-Nb-Zr-Ta system, electrochemical and biological properties were described and discussed for dentistry applications when coming into contact with the simulated biological fluid, and also with the cells hDPSCs and MG63.

The microstructural characterization showed that the as-cast TNZT alloy was formed by the β phase as its majority phase and with low α'' phase content. The elastic modulus is lower than other alloys, such as Ti-6Al-4V, which approaches that of bone and reduces the risk of final implant failure from inadequate stress shielding. Regarding its chemical characteristics, this alloy offers better corrosion resistance to Ti-6Al-4V and the worst condition compared to CP-Ti fabricated at the same condition. Furthermore, very few ions are released from all four elements of this alloy (Ti, Nb, Zr, Ta) while immersed in artificial saliva. Its data stands out compared to the Ti-6Al-4V alloy, given the considerable Al release, an element that is under study for possibly damaging the nervous system. Given the significant differences between the as-cast TNZT grain sizes and the β phase content compared to CP-Ti and Ti-6Al-4V, we evidenced that this characteristic can influence electrochemical mechanisms. Cytotoxicity assays demonstrate the TNZT alloy's noncytotoxicity or negative effect in a short time, related to the ion release, microstructure or chemical composition of the alloy. Furthermore, osteogenic differentiation of cells hDPSC in the obtained as-cast TNZT samples occurs. Marked cell adhesion takes place on sample surfaces. The behavior of these cells in contact with the alloy enables estimations to be made of how the bone-implant interface can act by promoting the area's regeneration, increasing the implant's success rate and reducing peri-implantitis prevalence.

In this way, the TNZT alloy's biocompatibility was proven and the reasons why it should continue to be an option were analyzed for its use in the biomedical field.

Author Contributions: Conceptualization, B.N.V., M.C.R. and V.A.B.; methodology, B.N.V., V.A.B. and L.M.; investigation, B.N.V., V.A.B. and A.V.E.; resources, V.A.B. and A.V.E.; writing—original draft preparation, B.N.V. and M.C.R.; writing—review and editing, M.C.R., V.A.B. and L.M.; supervision, V.A.B. and L.M.; project administration, V.A.B. and L.M.; funding acquisition, V.A.B. All authors have read and agreed to the published version of the manuscript.

Funding: The authors thank the Spanish Ministerio de Economía y Competitividad for Research Project RTI2018-097810-B-I00 and the European Commission for FEDER funds.

Conflicts of Interest: The authors declare no conflict of interest.

References

1. Gil, F.J. Aplicaciones biomédicas de titanio y sus aleaciones. *Biomecánica* **1993**, *1*, 34–42. [CrossRef]
2. Hanawa, T. Review: A comprehensive review of techniques for biofunctionalization of titanium. *J. Periodontal Implant Sci.* **2011**, *41*, 263–272. [CrossRef] [PubMed]
3. Kuroda, D.; Niinomi, M.; Morinaga, M.; Kato, Y.; Yashiro, T. Design and mechanical properties of new β type titanium alloys for implant materials. *Mater. Sci. Eng. A* **1998**, *243*, 244–249. [CrossRef]
4. Femenia, J.L.; Amigó, A.; Escuder, A.V.; Segovia, F.; Borrás, V.A. Desarrollo de las aleaciones de titanio y tratamientos superficiales para incrementar la vida útil de los implantes. *Rev. Metal.* **2016**, *52*, 84. [CrossRef]
5. Abdel-Hady, M.; Hinoshita, K.; Morinaga, M. General approach to phase stability and elastic properties of β-type Ti-alloys using electronic parameters. *Scr. Mater.* **2006**, *55*, 477–480. [CrossRef]
6. Pevida, E.P. Análisis Biomecánico de la Influencia del Material de Fabricación de Implantes Dentales en la Transferencia de Carga al Terreno de Soporte. Ph.D. Thesis, Universidad de Zaragoza, Zaragoza, Spain, 2017.
7. Kim, K.M.; Kim, H.Y.; Miyazaki, S. Effect of Zr Content on Phase Stability, Deformation Behavior, and Young's Modulus in Ti–Nb–Zr Alloys. *Materials* **2020**, *13*, 476. [CrossRef]
8. Zhang, T.; Ou, P.; Ruan, J. Nb-Ti-Zr alloys for orthopedic implants. *J. Biomater. Appl.* **2020**, *35*, 1284–1293. [CrossRef]
9. Mishchenko, O.; Ovchynnykov, O.; Kapustian, O.; Pogorielov, M. New Zr-Ti-Nb Alloy for Medical Application: Development, Chemical and Mechanical Properties, and Biocompatibility. *Materials* **2020**, *13*, 1306. [CrossRef] [PubMed]
10. Cordeiro, J.M.; Beline, T.; Ribeiro, A.L.R.; Rangel, E.C.; da Cruz, N.C.; Landers, R.; Faverani, L.P.; Vaz, L.G.; Fais, L.M.G.; Vicente, F.B.; et al. Development of binary and ternary titanium alloys for dental implants. *Dent. Mater.* **2017**, *33*, 1244–1257. [CrossRef]

11. Ozan, S.; Lin, J.; Li, Y.; Zhang, Y.; Munir, K.; Jiang, H.; Wen, C. Deformation mechanism and mechanical properties of a thermomechanically processed β Ti-28Nb-35.4 Zr alloy. *J. Mech. Behav. Biomed. Mater.* **2018**, *78*, 224–234. [CrossRef]
12. Cossú, C.M.F.A.; Vicente, E.D.; Cardoso, I.G.R.; Schettini, Y.S.; Precioso, J.A.G.; Nunes, C.A.; de Almeida, L.H.; Borborema, S. Mechanical and Microstructural Characterization of AS-CAST Ti-12Mo-xNb Alloys for Orthopedic Application. *Mater. Res.* **2020**, *22*. [CrossRef]
13. Ma, X.-L.; Matsugi, K.; Xu, Z.-F.; Choi, Y.-B.; Matsuzaki, R.; Lin, Z.-F.; Liu, X.-G.; Huang, H. Possibility of As-Cast Applications on β-Type Titanium Alloys Proposed in the Newly Expanded Area of Bot-Mdt Diagram. *Mater. Trans.* **2020**, *61*, 740–749. [CrossRef]
14. Rodrigues, I.R.; Lopes, R.E.L.; Grandini, C.R. Development of Novel As-Cast Ti-Mo-Zr Alloys for Biomedical Applications. *Mater. Res.* **2021**, *24*. [CrossRef]
15. Miotto, L.N.; Fais, L.M.G.; Ribeiro, A.L.R.; Vaz, L.G. Surface properties of Ti-35Nb-7Zr-5Ta: Effects of long-term immersion in artificial saliva and fluoride solution. *J. Prosthet. Dent.* **2016**, *116*, 102–111. [CrossRef] [PubMed]
16. Lutterotti, L.; Matthies, S.; Wenk, H.R. MAUD: A friendly Java program for material analysis using diffraction. *IUCr Newsl. CPD* **1999**, *21*, 14–15.
17. Rubi, J.M.; Kjelstrup, S. Mesoscopic nonequilibrium thermodynamics gives the same thermodynamic basis to Butler−Volmer and nernst equations. *J. Phys. Chem. B* **2003**, *107*, 13471–13477. [CrossRef]
18. Brailovski, V.; Prokoshkin, S.; Gauthier, M.; Inaekyan, K.; Dubinskiy, S.; Petrzhik, M.; Filonov, M. Bulk and porous metastable beta Ti-Nb-Zr(Ta) alloys for biomedical applications. *Mater. Sci. Eng. C* **2011**, *31*, 643–657. [CrossRef]
19. Brizuela, A.; Herrero-Climent, M.; Rios-Carrasco, E.; Rios-Santos, J.V.; Pérez, R.A.; Manero, J.M.; Gil Mur, J. Influence of the Elastic Modulus on the Osseointegration of Dental Implants. *Materials* **2019**, *12*, 980. [CrossRef] [PubMed]
20. Nelson, H.G. Environmental hydrogen embrittlement of an α-β titanium alloy: Effect of hydrogen pressure. *Metall. Trans.* **1973**, *4*, 364–367. [CrossRef]
21. Tal-Gutelmacher, E.; Eliezer, D.; Eylon, D. The effects of low fugacity hydrogen in duplex-and beta-annealed Ti–6Al–4V alloy. *Mater. Sci. Eng. A* **2004**, *381*, 230–236. [CrossRef]
22. Nelson, H.G.; Williams, D.P.; Stein, J.E. Environmental hydrogen embrittlement of an α-β titanium alloy: Effect of microstructure. *Metall. Trans.* **1972**, *3*, 469–475. [CrossRef]
23. Wipf, W.; Kappesser, B.; Werner, R. Hydrogen diffusion in titanium and zirconium hydrides. *J. Alloys Compd.* **2000**, *310*, 190–195. [CrossRef]
24. Shih, D.S.; Birnbaum, H.K. Evidence of FCC titanium hydride formation in β titanium alloy: An X-ray diffraction study. *Scr. Metall.* **1986**, *20*, 1261–1264. [CrossRef]
25. Hon, Y.-H.; Wang, J.-Y.; Pan, Y.-N. Composition/phase structure and properties of Titanium–Niobium alloys. *Mater. Trans.* **2003**, *44*, 2384–2390. [CrossRef]
26. Niinomi, M. Mechanical properties of biomedical titanium alloys. *Mater. Sci. Eng. A* **1998**, *243*, 231–236. [CrossRef]
27. Craig, R.G.; Peyton, F.A. The microhardness of enamel and dentin. *J. Dent. Res.* **1958**, *37*, 661–668. [CrossRef]
28. Maity, T.; Balcı, Ö.; Gammer, C.; Ivanov, E.; Eckert, J.; Prashanth, K.G. High pressure torsion induced lowering of Young's modulus in high strength TNZT alloy for bio-implant applications. *J. Mech. Behav. Biomed. Mater.* **2020**, *108*, 103839. [CrossRef] [PubMed]
29. Fong, H.; Sarikaya, M.; White, S.N.; Snead, M.L. Nano-mechanical properties profiles across dentin–enamel junction of human incisor teeth. *Mater. Sci. Eng. C* **2000**, *7*, 119–128. [CrossRef]
30. He, L.H.; Fujisawa, N.; Swain, M.V. Elastic modulus and stress–strain response of human enamel by nano-indentation. *Biomaterials* **2006**, *27*, 4388–4398. [CrossRef] [PubMed]
31. Habelitz, S.; Marshall, S.J.; Marshall, G.W., Jr.; Balooch, M. Mechanical properties of human dental enamel on the nanometre scale. *Arch. Oral Biol.* **2001**, *46*, 173–183. [CrossRef]
32. Garcia-Ramirez, M.J.; Lopez-Sesenes, R.; Rosales-Cadena, I.; Gonzalez-Rodriguez, J.G. Corrosion behaviour of Ti-Ni-Al alloys in a simulated human body solution. *J. Mater. Res. Technol.* **2018**, *7*, 223–230. [CrossRef]
33. Kelly, E.J. Electrochemical behavior of titanium. *Mod. Asp. Electrochem.* **1982**, *14*, 319.
34. Hanawa, T. Metal ion release from metal implants. *Mater. Sci. Eng. C* **2004**, *24*, 745–752. [CrossRef]